We are IntechOpen, the world's leading publisher of Open Access books Built by scientists, for scientists

4,800
Open access books available

122,000
International authors and editors

135M
Downloads

Our authors are among the

154
Countries delivered to

TOP 1%
most cited scientists

12.2%
Contributors from top 500 universities

CLARIVATE ANALYTICS BOOK CITATION INDEX INDEXED

WEB OF SCIENCE™

Selection of our books indexed in the Book Citation Index in Web of Science™ Core Collection (BKCI)

Interested in publishing with us?
Contact book.department@intechopen.com

Numbers displayed above are based on latest data collected.
For more information visit www.intechopen.com

20

Radargrammetric SAR image processing

Stéphane Méric, Franck Fayard and Éric Pottier
Institute of Electronics and Telecommunications of Rennes,
European University of Britanny
France

1. Introduction

Throughout history, humans have tried to represent what they see through images. Mapmakers have always sought ways in which to represent both the location and the three dimensional shape of land. At the beginning, the way to obtain a 3D representation of land was to measure planimetry and height (as we can identify later by longitude, latitude and height) using basic measuring devices. Nowadays, the improvements of airborne and spatial instruments make it possible to produce images by sensing the electromagnetic radiation from the Earth. So, we can distinguish two classes of remote sensors: optical sensors and radar sensors. Optical sensors, such as Landsat or SPOT 5, operate around the visible spectrum and provide images with a fine resolution (less than 5 meters for SPOT 5). Thus, these kinds of sensors become very useful for civilian applications (cartography, elevation map, agriculture, hydrography, management of natural hazards, meteorology, geology, deforestation and so on). Considering the subject of this chapter, the extraction of terrain elevation by stereoscopic images can give digital elevation models with an error of about 5 meters (Toutin, 2000). However, optical sensors could be critically useless because of weather conditions or lack of light (i.e. sun). Thus, the use of radar sensors is a good way to overcome the limitations of optical sensors: not very sensitive to rain, considered as active sensors (because they have their own source of energy). Thanks to the signal processing applied to radar signal (pulse compression and synthetic aperture), radar systems can provide images with a very high resolution (for example, Radarsat-2 has an ultra-high resolution mode of about 3 meters for resolution). So, radar images are considered as additional information to optical images. With regard to these properties, one can estimate that radar images are used to get elevation terrain. The more intuitive way to extract depth information from remote sensing images is stereogrammetry. As the brain operates on optical images from eyes, the technique of radargrammetry is applied to SAR (Synthetic Aperture Radar) stereo data and provides digital elevation models (DEM). Considering this preamble to the radargrammetric world, this chapter examines one way to produce digital elevation models (DEM) from a mountainous area (the French Alps) and the way to improve the accuracy of the DEM. So, we will organize the discussion in three parts. In part 1, in order to better understand the stereo computation, we need to explain the basic characteristics of a radar image, which is particularly important to be considered during the radargrammetric processing. Thus, a radar image can be seen as a distribution of reflected electromagnetic energy on the ground. So, each element (i.e. a pixel) of an image is described by its size along the azimuth and range axis. Also, specific characteristics of a radar image are described as layover, shadowing and foreshortening. Because radargrammetric processing is

based on fitting images, we need to establish a common reference to radar images and to set up geographical coordinates for each image. Considering the position of the sensor, we can establish rigorous radar projection equations that can be compared to the so-called photogrammetric equations. As the radiometry is important to interpret a radar image, we consider the main radiometric models and the speckle phenomenon considered as noise in the SAR image. In part 2, considering a radar image, we will present the basic operations of extraction from satellite radar data. There are several methods to reconstruct elevation model from radar images. These images are essentially described as 2D information. So, one has to extrapolate 3D information from 2D description (as DEM). There are different methods to do this: clinometry, stereoscopy, interferometry and polarimetry. Since any sensor, system or method has its own advantages and disadvantages, the choice of a radargrammetric technique depends on the sensors and the means used during image acquisition. For the stereoscopic method, the capability of radar image pairing to achieve radargrammetic processing depends on geometric configuration in relation with the radar trajectory. Considering this radar trajectory, one can define the radar stereo base, the intersection angle and the parallax. We propose to review different ways to process the matching operations. These ways are correlation operations based upon searching for match points as area correlation methods or elementary correlation. After that, we will expose some improvements in the matching process (pyramidal scheme, speckle filtering). Part 3 will deal with the description of radargrammetric applications on real data (from SIRC shuttle mission) and the different steps to obtain a DEM. First of all, we describe the radar image and especially the relations between the satellite route and the ground radar image. This step is crucial in order to efficiently match the stereo radar images. Also, we explain the significance of using ground control points (GCPs) to rectify radar images. The next step is the matching operation between the two stereo SAR images. It consists in determining the point co-ordinates inside the secondary image for each point in the reference image, which is called the corresponding pixel. The computation of the 2D normalized cross-correlation coefficient is used on SAR images. At this step, we use a hierarchical strategy to reduce process time and use a filter to get the high accuracy disparity map. Then, we apply the rigorous radar stereo intersection problem and compute the stereo radargrammetric equations. Using the solutions, we obtain a DEM from the stereo radar images. This DEM is compared with a reference DEM. At the end, we move on to the point of improvement of the DEM: obvious improvements (correction of incoherent points) and further improvements in progress (use of adaptive correlation windows or polarimetric parameters).

2. Radargrammetric sensors

2.1 Introduction

As the acronym RADAR means “Radio Detection and Ranging”, the basic principles are to detect and range objects located in front of the radar system. In the context of remote sensing, a scene (i.e. the terrain) is considered to be imaged by transmitting an incident electromagnetic wave from the radar, reflecting towards the radar (monostatic consideration) and receiving the reflected wave.The radar signal is obtained through the conversion of an electrical current on the antenna surface induced by an electromagnetic field around this antenna and vice-versa. Thus, the received signal contains information about the scene such as dielectric properties. Firstly, we can describe the received power P_r through the radar equation:

$$P_r = \frac{P_t.G^2.\lambda_c^2}{(4\pi)^3 R^4}\sigma$$

where P_t is the transmitted power, G is the gain of the transmitted and received antenna, λ_c is the wavelength of the transmitted wave, R represents the distance between the radar and the scene and σ is the radar cross section. This parameter depends on many parameters such as the frequency and polarisation state of the emitted wave, the dielectric nature of the object, geometrical body of the object and so on. For example, buildings forming a corner with the ground or other buildings, correspond to high reflected energy. Conversely, roughness surfaces diffuse the incident energy and correspond to low reflected energy.

2.2 Signal processing and radar imaging

The side looking aperture radar (see figure 1) makes it possible to get radar images of the ground by emitting pulses of electromagnetic waves. The platform (aircraft or satellite) of

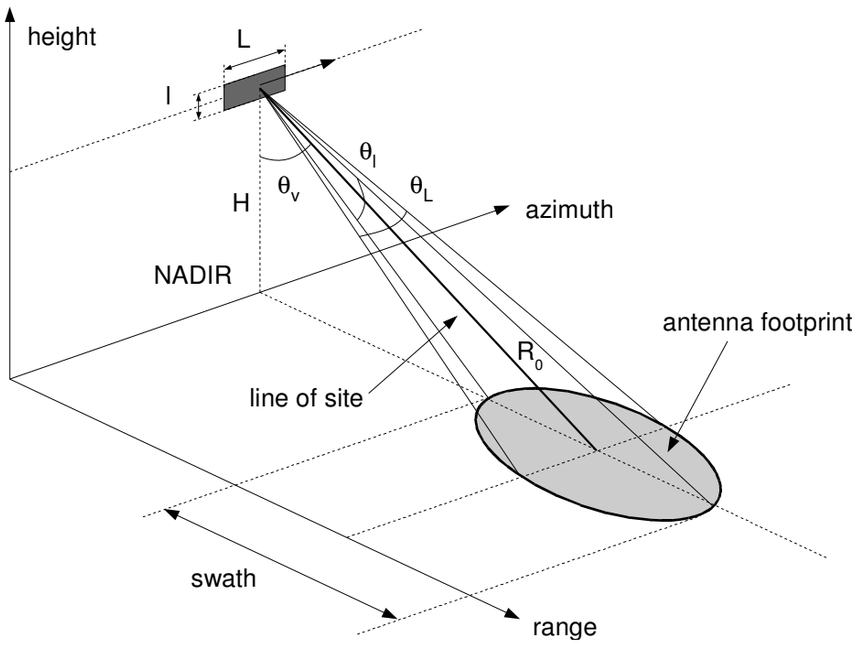

Fig. 1. Configuration of side-looking

such a radar travels forward in the flight direction or along-track (azimuth axis) with the nadir directly beneath the platform which is at the height H. The range axis refers to the across-track dimension perpendicular to the flight direction. The microwave beam is transmitted obliquely (elevation angle θ_v to the direction of flight illuminating a swath. The side looking geometry is necessary to avoid the Doppler ambiguity. Some configurations exhibit a squint angle rather than an antenna pointing perpendicularly to the flight direction. The footprint of the antenna is defined through the line of sight of the main beam of the antenna and the aperture angles (along the range and azimuth axis) of this antenna. This aperture angle refers to the physical dimension of the antenna (respectively l and L). Swath width refers to the strip of the Earth's surface from which data is collected by the radar. The longitudinal extent of the swath is defined by the motion of the aircraft with respect to the surface, whereas the swath width is measured perpendicularly to the longitudinal extent of the swath.

2.2.1 Processing the image

This chapter presents results from data obtained by a pulse radar. The word "resolution" means the precision to which we can measure the location of a point target and not necessary the capability of the radar to distinguish two targets (volume of confusion). Also, we can define the unfocused resolution along the range axis $\delta_d = c\tau/2$ and along the azimuth axis δ_a which partially depends on the value of R_0. At each position for the radar, an electromagnetic pulse is emitted with the period repetition commonly known as the inverse of the pulse repetition frequency (PRF). The pulse duration is very brief compared with the period of repetition. Thus, the reflected signal is recorded during almost the period repetition minus the pulse duration. The time of the beginning of the recorded signal is called t_p and the end is referred t_d. Also, we can define the physical limit of the radar image which is processed in the slant plane (see figure 2)

- the near range $R_p = (c.t_p)/2$,
- the far range $R_d = (c.t_d)/2$.

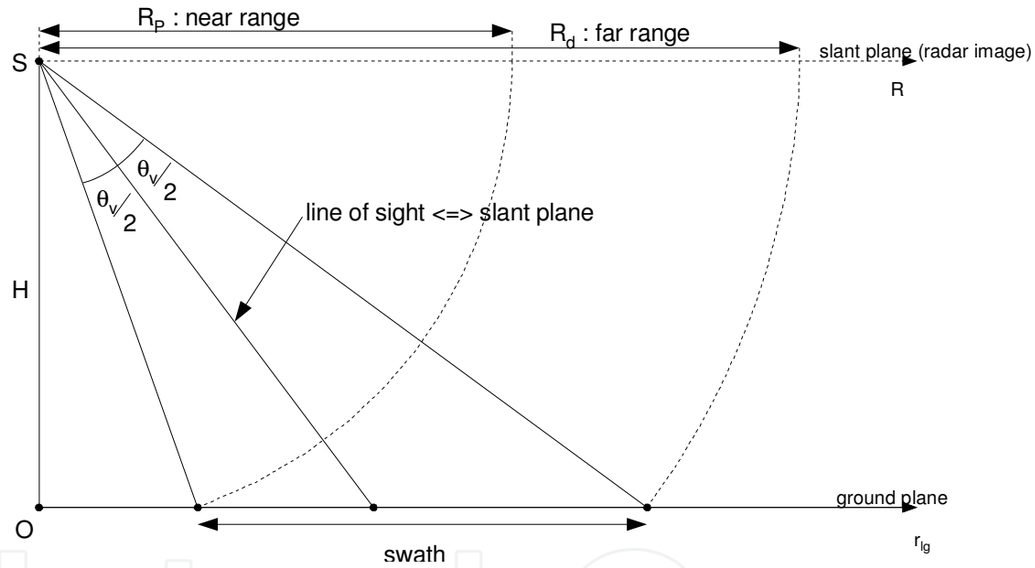

Fig. 2. Projection to the slant plane and to the ground plane

In order to get a ground-plane radar image, we have to interpole and resample the slant-plane radar image and be sure that the range resolution is constant along the range axis. Ground-plane imagery must be obtained with minimal distortion if comparisons with maps taken from other sensors (for example sensors) are needed.

2.2.2 Range resolution

Actually, the term SAR refers to signal processing that improves the azimuth resolution. Considering the parameters of the SIR-C mission, the pulse duration is equal to 33.8 μs and the resulting range resolution is more than 30 kilometers,which is unacceptable for remote sensing applications. Fine resolution is achieved by transmitting and receiving frequency modulated radar waves. The modulation is characterized by a wide bandwidth B_p. The echo is processed

by a matched filter that fine tunes the range resolution δ_d:

$$\delta_d = \frac{c}{2.B_p}$$

Thus, the range resolution is inversely equal to the bandwidth of the emitted signal. Therefore, using the parameters of the SIR-C mission and especially the value of B_p (10 Mhz), we can get a range resolution of about 15 meters.

2.2.3 Azimuth resolution

Crossrange resolution is naturally achieved by use of an antenna with a narrow beam and specified by θ_L. If the beamwidth along the crossrange axis is given approximately by $\theta_L \approx \lambda/L$ where λ is the wavelength of the transmitted signal , the corresponding azimuth resolution δ_a at range R_0 is then $\delta_a = \lambda.R_0/L$. Considering the SIR-C mission again, the azimuth resolution would be about 30 kilometers, which is also unacceptable. The synthetic aperture processes the received signal by using the fact that the radar views the scene from slightly different angles. These different views (at each emitted pulse) are obtained because the radar moves through its synthetic aperture. Considering the response of one point on the ground, the reflected signal from this point can be seen as a frequency modulated signal (Doppler frequency). Also, a matched filtering operation is applied along the azimuth axis under certain assumptions (width of Doppler spectrum and duration of the seen point), we write the azimuth resolution δ_a as

$$\delta_a = \frac{L}{2}$$

which gives an azimuth resolution of 6 meters considering the characteristics of the antenna of the shuttle (SIR-C).

2.2.4 Radar image corrections

The values of resolution given above are usually better than those obtained by the real system. Also, the signal processing must take into account undesirable effects that affect the performances of the radar. Concerning our discussion about radargrammetry, we can note among these effects:

- the range migration that can be modelled by the parabolic variation of the distance between the target point on the ground and the radar along the synthetic aperture (this point is corrected by different processing methods (Carrara et al., 1995)),
- the radiometric variations due to the change of received signal power from the beginning of the swath (near range) to the end of the swath (far range) for each position of the radar (using well-known ground points as RCS references can correct this effect),
- the motion compensation that corrects the deviation of the antenna from its nominal flight path.

Despite the corrections, some errors such as bad localization of pixels can still be found on the radar image. These errors can finally be eliminated by making use of ground control points such as buildings, cross-roads, mountain tops and so on.

2.3 Geometric interpretation of a SAR image

Actually, the importance of geometry for the interpretation of radar images recurs throughout this chapter. As we wrote before, the radar system can be considered as an Èall-weatherÉ system and contrary to optical imagery, does not need ambient light or an external source of energy to obtain images. However, upon comparing a SAR image and an optical image, we can assume that certain properties of an optical image are not included in the radar image. For example, this phenomenon is clearly visible when looking at pixels farther from the radar, which appear smaller along the range axis than pixels closer to the radar. Although the cross range resolution is not affected by the radar imagery process, we suppose that the relief of the terrain will induce radiometric and, especially, geometric distortion. Thus, if we consider a ground point with a height h and located at a range R from the radar at the height H, the position x_{sol} along the range axis is given by:

$$x_{sol} = \sqrt{R^2 - (H-h)^2}$$

and means that a single radar image doesn't give the altitude of a pixel but must be associated to a height model of the terrain. This is one of the tricky points about the interpretation of a radar image.

2.3.1 Distortion of a radar image

The projection of a terrain slope on the slant range of the radar induces well-known distortion that can be expected as regards the planimetry (see figure 3). And, the values of resolution

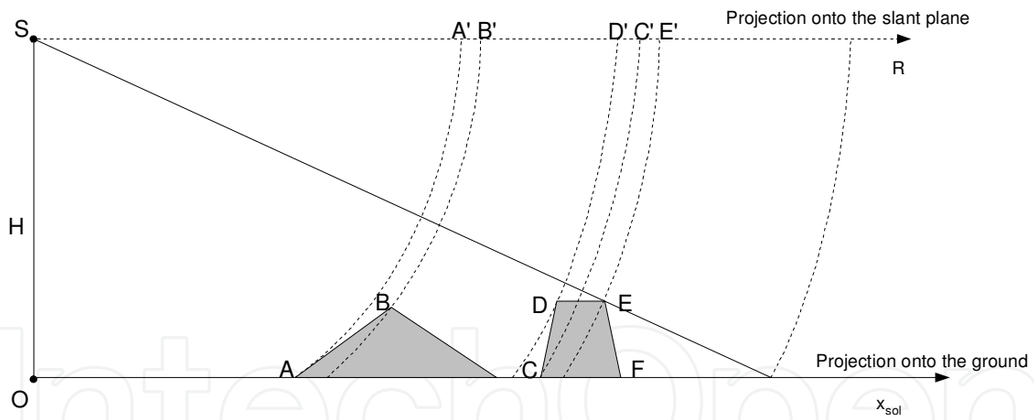

Fig. 3. Geometrical distortion occurs in the slant radar image.

given above are usually better than those obtained by the real system. Also, the signal processing must take into account undesirable effects that affect the performances of the radar. Concerning our discussion about radargrammetry, we can note among these effects the foreshortening effect, the layover effect and the shadowing effect which result from relief displacement.

2.3.2 Foreshortening effect

The foreshortening effect occurs when the radar beam reaches the base of a slope tilted towards the radar before the top of this same slope. The straight segment [AB] and its image [A'B'] onto the slant range illustrate this effect in figure 3. Thus, the radar measured distance

seems to be shorter than the real one and this effect is maximum when the radar beam is perpendicular to the mountain slope.

2.3.3 Layover effect

The layover effect occurs when the radar beam reaches the top of a mountain or a hill before its base. The straight segment [CD] and its image [C'D'] onto the slant range illustrate this effect in figure 3. Also, a terrain slope towards the radar produces a viewing permutation between the top and the base of a mountain on a radar image.

2.3.4 Shadowing effect

The shadowing effect occurs when the radar beam is not able to illuminate the radar scene. This effect that can be seen in figure 3 considering the straight segment from the point E', image of the point E, to the end of the swath. Also, the radar shadow is considered as an optical shadow and induces a black area on the radar image because no reflected wave comes from this kind of region (for example, point F is not seen on the radar image). All these effects are quite severe in order to understand a radar image well and especially in mountainous areas. Moreover, the incidence angle of the radar beam is another important parameter to estimate the influence on the interpreted radar image. So, the efficiency of the radargrammetric processing must take into account these characteristics.

2.3.5 Geometrical model of the radar position

The capabilities to link each pixel of a radar image to a real position on the terrain is one of the most important steps of the radargrammetric processing because correction, rectification, resizing and superimposition processings of the image need to know the geometrical position of a pixel. The model of the platform (e.g. in our study a satellite) flight path is described in figure 4 provides relation between radar image indexes and the terrain (Girard, 2003) thanks to

- radar parameters (frequency, size of the antenna, incidence angle ...),
- instantaneous position and motion of the radar platform,
- an ellipsoidal model of the Earth.

For the last item, the figure 4 gives several parameters to describe the model as

- angles λ and ϕ which are respectively the longitude position and the latitude position,
- Earth's referential (G,i,j,k) which is established by the centre of the Earth G, the i-axis towards the Greenwich meridian, the k-axis coinciding with the Earth's axis of rotation and the j-axis forming a right-handed system with i-axis and k-axis instantaneous position and motion of the radar platform,
- referential of satellite (S,l,r,t) linked to the satellite and described by the position S of the satellite, the l-axis colinear to the vector $\vec{GS}$, the t-axis simultaneously perpendicular to the l-axis and the vector $\vec{S}$ and the r-axis forming a right-handed system with l-axis and t-axis.

As described in (Dhond & Aggarwal, 1989), stereoscopic processing needs to know several parameters which corresponds, for radargrammetry processing, to:

- the wavelength λ_c of the transmitted wave,
- the azimuth resolution δ_a and the range resolution δ_d,

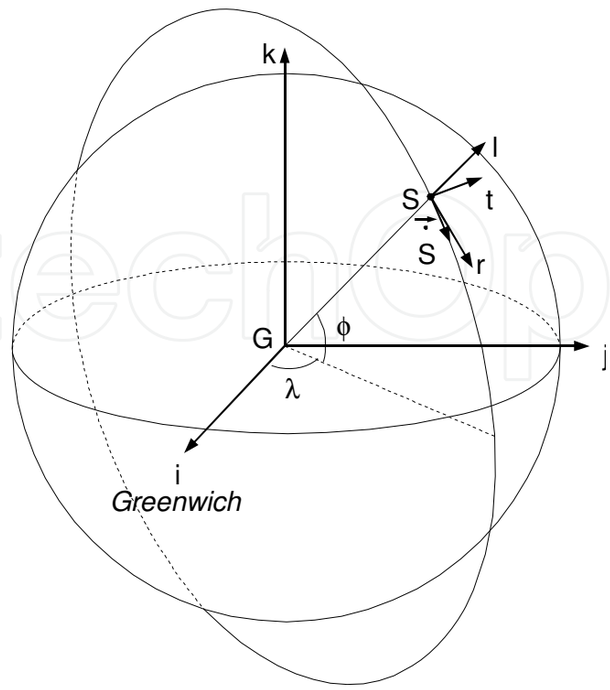

Fig. 4. Position and motion of a satellite

- the central Doppler frequency f_D of the received signal,
- the time t_0 for which the values of the position and the velocity of the satellite are known,
- the initial time t_{init} of the beginning of the radar image,
- the range distance r_0 given for a reference line of the image,
- parameters that make it possible to calculate the behaviour of the satellite (position, orientation, velocity) for each value of time.

Actually, the position and velocity of the satellite are known at specific values of time which are called ephemerides. Thus, we have to interpolate the path of the satellite in order to have all the position and velocity of the satellite along the flight path.

2.3.6 Geographic coordinates of a radar image

Thanks to the parameters describing the flight path of the satellite, it is possible to give geographic information for each pixel of the radar image. In order to establish this relation and to measure locations accurately, some references of coordinates are used (Dufour, 2001). In this chapter, we use the global coordinate system which has been described before (see figure 4). The ellipsoidal height h of a point is the vertical distance of the point in question above the reference ellipsoid. The reference ellipsoid is described by the WGS84 system (geodetic) and the significant parameters defined by

- the semi-major axis $a = 6378137.0$ meters,
- the semi-minor axis $b = 6356752.3$ meters.

Considering a point M defined by its height h and its geocentric coordinates (x,y,z) in the (G,i,j,k) reference, we can write the above expression:

$$\frac{x^2+y^2}{(a+h)^2}+\frac{z^2}{(b+h)^2}=1$$

2.3.7 Radar coordinates and image coordinates

In the radar reference, each pixel of the image gives information about the range distance r and the time t elapsed since the beginning of the recorded raw data. Another way to describe a radar image refers obviously to the azimuth u and range r coordinates. Also, a data transformation is feasible via the number of looks N_f used to establish the radar image (Curlander, 1991) and the spatial sampling frequency f_e along the range axis:

$$\begin{cases} t &= \frac{N_f}{f_r}.u+t_{init} \\ r &= \frac{c}{2f_e}.v+r_0 \end{cases}$$

We have to note that the values of u and v are immediately obtained from the radar image. At this time, we have to set up the coordinates t and r in the defined Earth's reference.

2.3.8 Range sphere and Doppler cone

We can define the range sphere as the constant distance r of a point M from the radar located at the position S:

$$|\overrightarrow{SM}|=r$$

Moreover, the Doppler cone is the cone of equal Doppler frequency and has its apex located at the centre of the range sphere:

$$f_D=\frac{2}{\lambda_c}.\frac{\vec{S}.\overrightarrow{SM}}{|\overrightarrow{SM}|}$$

In the case of side-looking radar, the centroid Doppler frequency f_D is equal to zero, which means the cone becomes a plane perpendicular to the velocity vector $\overrightarrow{SM}$. Considering the coordinates

- (x,y,z) of the point M on the radar image,
- (X_S,Y_S,Z_S) of the position S of the radar,
- $(\dot{X}_S,\dot{Y}_S,\dot{Z}_S)$ of the velocity of the radar,

the equations 2.3.8 and 2.3.8 establish a system of 2 equations of 3 unknowns (x,y,z) whose solutions describe a circle called Doppler circle (see figure 5). The Earth's model as defined before and raised of height h_e finally makes it possible to get two solutions of the given system. One of these can be eliminated considering the line of site (LOS) (figure 6). Unfortunately, the different slopes of terrain above the Earth's ellipsoid that we described before and the associated effects (especially in foreshortening areas) on the radar image result in more than one solution.

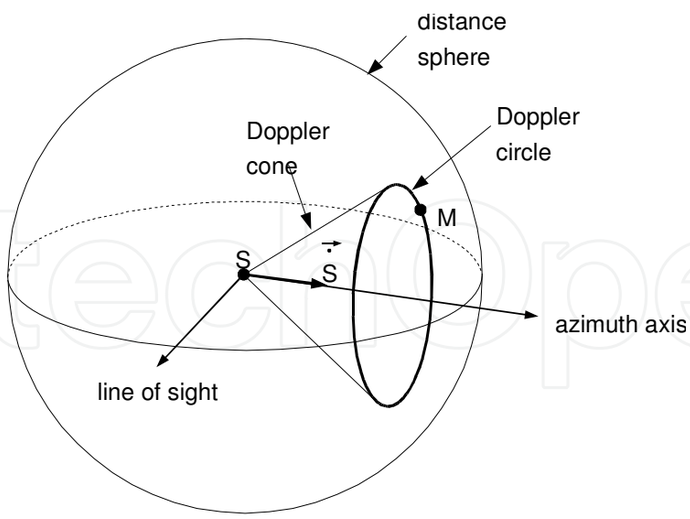

Fig. 5. Description of the distance sphere, Doppler cone and Doppler circle

2.4 Radiometric phenomena in an SAR image

The first remark concerns the main difference between the radar image and the optical image. The Earth's surfaces reflecting strong energy towards the radar correspond to very bright pixels on the radar image (and can appear dark on an optical image). The radar scene reflects a certain amount of radiation according to its geometrical and physical characteristics. This part will deal with radiometric phenomena that occur on the ground and which essentially depend on the electrical properties of the soil and the roughness of the area. Moreover, as we have seen before, the geometric shape of an area or an object on the ground mainly determines the radiometry of a pixel and the brightness of a feature could be a combination with other objects. Another important parameter is the wavelength of the incident radiation wave and the electromagnetic interaction falls with either surface interaction or volume interaction. Also, we can separate the interactions into two main topics:

- smooth surfaces that reflect (nearly) all the incident waves towards to a particular direction: specular reflection. If the surface is tilted towards the radar, the corresponding radar image appears very bright. Conversely, if the surface is not turned towards the radar (e.g. calm water or paved roads), the surface appears dark on the radar image;
- rough surface that scatters the incident wave in many directions: diffuse reflector.

In order to determine the degree of roughness of a surface, we use to establish (Beckman & Spizzichino, 1987) a relation between the state of the surface quantified by the average height variation h, the wavelength of the wave λ_c and the local incidence angle θ_i (see figure 7). This relation is known as the Rayleigh criterion:

$$\begin{cases} h < \dfrac{\lambda_c}{8\cos\theta_i} \text{ lorsque } \lambda_c \gg h \\ h < \dfrac{\lambda_c}{32\cos\theta_i} \text{ lorsque } \lambda_c \simeq h \end{cases}$$

Let us consider the local incidence angle: an incidence angle is the angle between the radar beam and the target object. The value of this angle determines the radar appearance of this

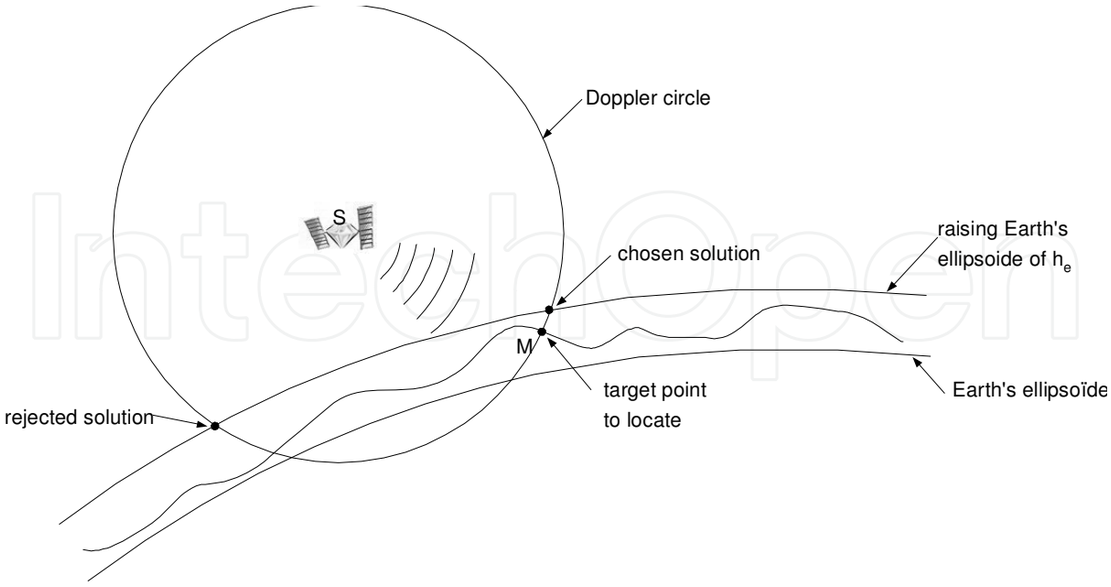

Fig. 6. Intersection of the Doppler circle and the Earth's surface

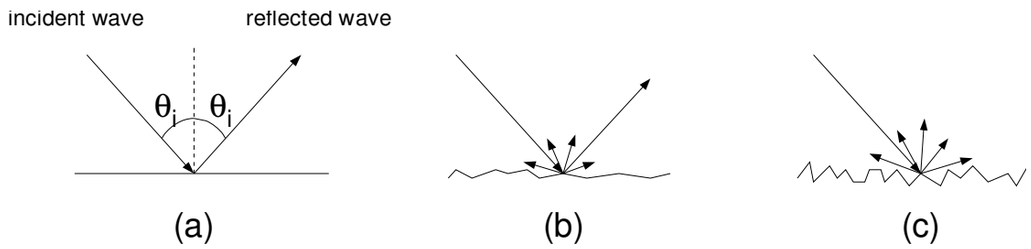

Fig. 7. Rayleigh criterion: (a) smooth surface, (b) low roughness surface and (c) high roughness surface

target on the radar image. Moreover, we can attach to each pixel of the radar image a local incidence angle so that we can notice variations in pixel brightness concerning one target object (rocks, trees, grass, buildings). Finally, we can note that the variation of incidence angles is less for a satellite radar than an airborne radar because of the height of the platform. Among the natural Earth's surfaces, we can characterize (Ulaby, 1981) three kinds of surface

- bare surface where simple reflections occur and the amount of energy towards the radar depends on the roughness of the soil,
- farmed surface where reflections are quite complex and depend on the crops, the moisture, the direction of the parcels and so on,
- vegetation surface where the reflection phenomena essentially depend on the wavelength. For example, the waves of the radar band X are only reflected by the top of the canopy. Lower wavelength waves penetrate the canopy and volume scattering has to be considered. Finally, some features on the ground can be considered as close targets,which means these features have two (or more) surfaces (generally smooth) forming a right angle and cause double (or more) bounce reflections (figure 8).

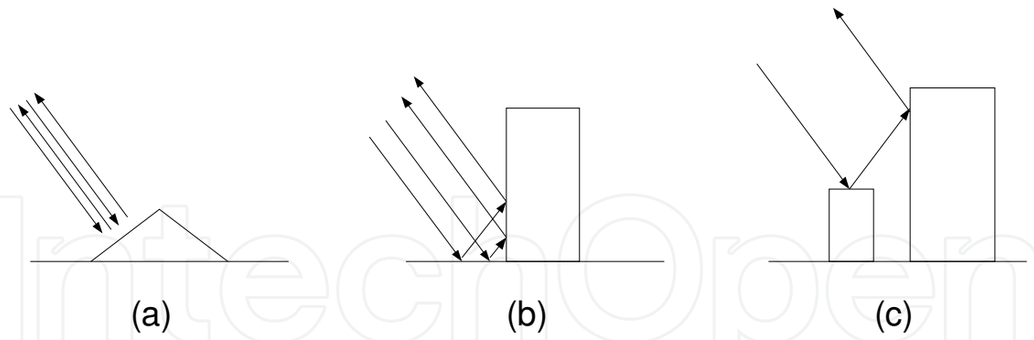

Fig. 8. Reflection phenomena: (a) from slope towards the radar, (b) from corner reflector (double bounce reflection) and (c) multiple bounce reflections.

The typical occurrence of this phenomenon is the corner reflection. Corner reflectors are very common in urban sites and show up as very bright targets on the radar image.

2.4.1 Speckle phenomena

As the radar image is created through a radar coherent wave, a particular effect modifies the radiometry of pixels as a noise-like effect inherent in coherent imaging systems. This effect is obviously visible on large covered-grass areas and looks like a "salt and pepper" texture. This texture is due to the chaotic response of multiple small targets on the ground whose global response is seen as a constructive or destructive random process. Thus, this kind of process randomly produces bright and dark pixels: the radar image is speckled. Many articles are dedicated to the study of the speckle phenomena (Goodman, 1976). Even it could be considered as information for special applications, the speckle effect is seen as a multiplicative noise and degrades the quality of a radar image.

3. Radargrammetric operations

3.1 State-of-the-art

The definition of radargrammetry has been stated by Leberl (Leberl, 1990): “Radargrammetry is the technology of extracting geometric information from radar images”. To extract the geometrical characteristics of the ground, four different techniques are implemented: stereoscopy, clinometry (Horn, 1975), interferometry (Massonet & Rabaute, 1993) and polarimetry (Schuler et al., 1996). These are usually combined with SAR systems which have been briefly presented in this paper. Because the aim of this chapter is only to expose the radargrammetry as a radar stereoscopic method, the other ones will not be more developed. The first works on radargrammetry began after the Second World War and the first principles were defined by La Prade (La Prade, 1963). These works were completed by several mathematical developments (Gracie et al, 1970) and fully developed by numerous researchers (Rosenfeld, 1968) (Leberl, 1990) (Polidori, 1997). All of these developments were tested and improved thanks to several operational measurements both airborne (for example (Azevedo, 1971) mapping the world’s tropical belt) and spatial (for example (Schrier, 1993) geocoding radar images from ERS-1 mission). Since the 1980s with the Shuttle Imaging Radar (SIR-A, SIR-B and especially SIR-C), the European satellite (ERS-2 and ENVISAT), the Canadian sensor (RADARSAT-1 and 2), the number of researchers working on the radargrammetric topic has increased and data

analysis has become more sophisticated (various incident angles, various frequencies and polarisations of the wave and so on).

3.2 Basics of radargrammetry as a radar stereoscopic method

3.2.1 Principle

Stereoscopy is a viewing method that forces our eyes to see, at the same time, two images taken from different angles. This technique allows us to see in three dimensions as it reinforces physiological indicators. The indicators used by stereoscopic method are parallax and convergence angle and can be defined as follows:

- the parallax P of an observed point is a parameter that is directly connected to the point elevation and it increases with the altitude of the point,
- the convergence angle $\Delta\theta_v$ is defined by the intersection of the two lines of sight of the radar and this angle increases as the baseline B_s rises.

In figure 9, the same-side stereoscopic configuration is exposed and the description of the parallax P, the base-line B_s and the intersection angle $\Delta\theta_v = \theta_{v1} - \theta_{v2}$ is given. The latter parameters have an important function as regards the quality and the accuracy of the terrain reconstruction.

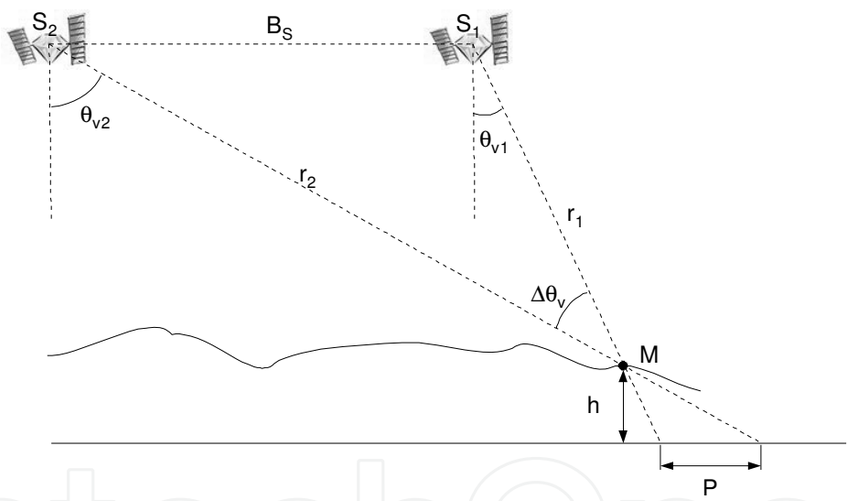

Fig. 9. One radar stereoscopic configuration.

3.2.2 Matching step

Stereoscopic techniques applied to radars are influenced by optical techniques (we can compare the baseline B_s in the radargrammetry configuration and the vertex in the human description), except that SAR images replace optical systems images. But, the main difficulty is to get used to new and unnatural radar viewing (as we exposed before) and especially when both geometric and radiometric disparities are large. However, radar images can be viewed in stereo after training. The point of radargrammetry is to match two radar images by a "registration" processing. The registration step aligns two images containing the same radar scene but viewed from different positions. The aim of the matching step is to get a dense description in order to achieve the accuracy of image registration. The main difficulty of the registering

operations comes from the dissimilarities between the pair of images that are caused by different imaging configurations. The identification of corresponding image points is the main feature of the processing. This step is generally achieved by using several methods and we will present two of them:

- grey-level image matching,
- edge-based method.

The first one is generally computed with the normalised cross-correlation coefficient (Leberl et al., 1994) and many improvements such as the use of the sum of mean normalised absolute difference or the least squares solutions are investigated. The second one is based on the fact that an object or a structure may look quite similar in both images whatever the radar position (Marr & Hildreth, 1980). However, this method needs some preprocessing (e.g. filtering operations) in order to be really efficient and the application to , for example, a mountainous area is not possible because of the small area of edges relatively to the total area of images. Thus, the combination of both methods can achieve good results (Paillou & Gelautz, 1999).

3.2.3 Disparity measurement and terrain reconstruction

For each pair of images, we get one map of disparities along both the azimuth axis and the range axis. In the case of a flat Earth, no disparity along the azimuth axis should occur when radar images come from parallel flight paths. But, because of the lack of precision of the radar trajectories, azimuth disparities exist and the way to eliminate these is to resample images into an epipolar geometry. At the end of the radagrammetric processing, the computation of a disparity map obtained under the flight conditions produces the terrain elevation which is called DEM (e.g. Digital Elevation Model). The calculated height of each pixel on the image agrees with the different equations describing the geometry of the flights of path. Moreover, in order to get a better DEM, the use of ground control points is essential to correct the geometric model of the terrain and to set up the best stereomodel as regards the solution of the stereo geometry.

3.3 Radargrammetric processing

As the radargrammetric method was briefly described in the late section, we intend to expose more precisely all the steps required to reach a terrain elevation thanks to a pair of stereo radar images.

3.3.1 Acquisition of stereo images

An important radar stereoscopic issue is the way measurements have to be made. Two main configurations can be considered: same-side (the radar is located on the same side considering the position of the two radars) and opposite-side (the scene is located between the two radars) viewing. Considering the same-side configuration (see figure 10), a large baseline (e.g. a large intersection angle) makes it possible to achieve good geometry for stereo plotting because of the increase in parallax values. And the higher the parallax value is, the more accurate the elevation reconstruction is. Conversely, the matching processing needs to manipulate images as closely identical as possible in order to succeed in stereo viewing. That implies a small intersection angle. The opposite-side configuration (figure 11) provides a large baseline and thus precise stereo plotting. Moreover, we can see in figures 11 and 10 the consequence of a range estimation error (the real point M migrates to the point M_e that is located by processing) that is less significant in the opposite-side case than the same-side one But, the radiometric differences are so important in the case of opposite-side configuration that the matching operation

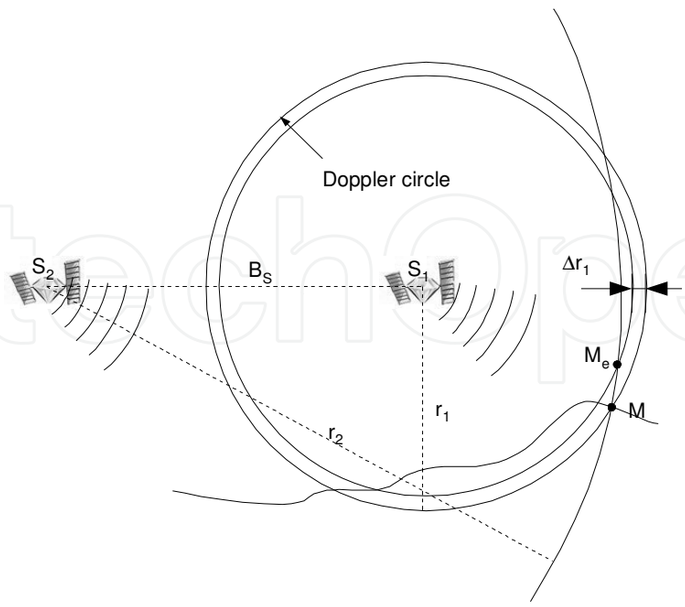

Fig. 10. Same-side configuration and range error consequence

is almost impossible without a preprocessing of images (for example, radiometric inversion). However, some studies (Toutin & Gray, 2000) demonstrate that we can have conflicting conclusions about theory developments and image applications. Anyway, the choice of the pairs of stereoscopic images comes up regarding the capability to get the parallax values and the accuracy of the height reconstruction. Thus, a compromise has to be reached between these two topics and concerns the baseline B_s to the height H of the platform ratio. This ratio can vary from 0.25 to 2. For example, a study about RADARSAT measurements (Sylvander et al., 1997) suggests an intersection angle of about 8° that corresponds to a value of B on H ratio equal about 0.3.

3.3.2 Correlation matching operation

The most common image matching method is area correlation. For a given area in the primary image, the matching computation has to detect the closest one in the secondary image by searching for the best matched area. The difference of position is the value of the parallax or disparity. The classical method of finding match areas is to use an analytical metric comparison and the zero-mean normalized cross-correlation (ZNCC) can be applied to searching for windows of radar images. These windows are usually squared and the size is (2n+1) by (2n+1) pixels, so a centre pixel can de defined. The ZNCC is often used because of robustness on the radiometric variations of the radar image and the result is given by the cross-correlation coefficient ρ. This coefficient ρ can be stated as follows:

$$\rho = \frac{E[I_1 I_2] - E[I_1]E[I_2]}{\sqrt{V(I_1)V(I_2)}}$$

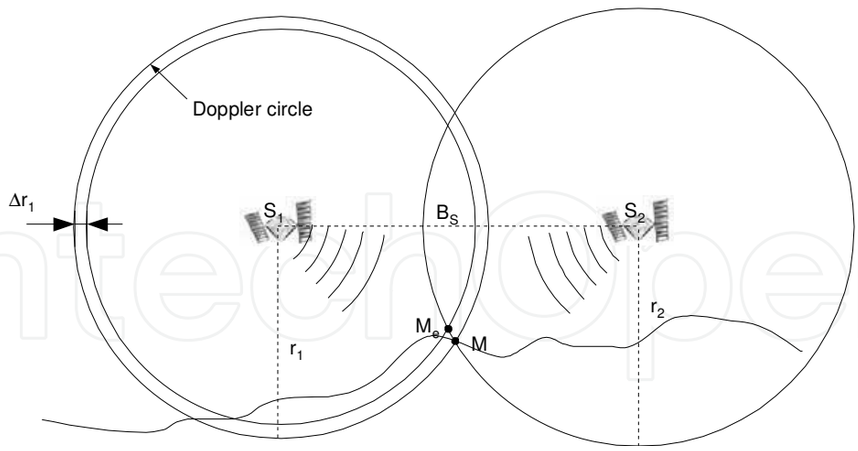

Fig. 11. Opposite-side configuration and range error consequence

where I_1 and I_2 represents the amplitude value of the pixels of the window. The mean or mathematical expectation $E[I_i]$ is calculated thanks the following expression:

$$E[I_{1,2}] = \frac{1}{N} \sum_{k=1}^{N} I_{1,2}^{k} \tag{1}$$

where N represents the number of pixels inside the window. Moreover, the variance expression $V(.)$ about the window I_i is given by:

$$V(I_{1,2}) = E[(I_{1,2} - E[I_{1,2}])^2] \tag{2}$$

The value of ρ is bounded by (-1) and (+1) and the windows are considered matched for the maximum value of ρ. The coefficient ρ is calculated for each position (az_s and rg_s) of the researching window in the researching area. Also, we get a correlation surface obtained with the values of the coefficient ρ and the maximum of this surface gives the disparity disp_{az} along the azimuth axis

$$\text{disp}_{az} = |az_s(\max) - az_r|$$

and the disparity disp_{rg} along the range axis

$$\text{disp}_{rg} = |rg_s(\max) - rg_r|.$$

This step is carried out for each point of the primary image in order to get the disparity map. The figure 12 illustrates the correlation computation applied for one pixel inside the primary image. Considering the assumptions of radiometric distortions in a radar image, the cross-correlation computation does not work very well on such degraded images (shadowing effect for example). That is the reason why the choices of the viewing configuration and the value of B_S are very important. Especially in mountainous areas, a large part of unmatched pixels can occur because of the shortening and layover effects. Finally, the choice of the greatest value of ρ for a given correlation computation is not necessarily the optimum criterion but must be considered with other parameters. Several methods can be applied to improve the matching operation.

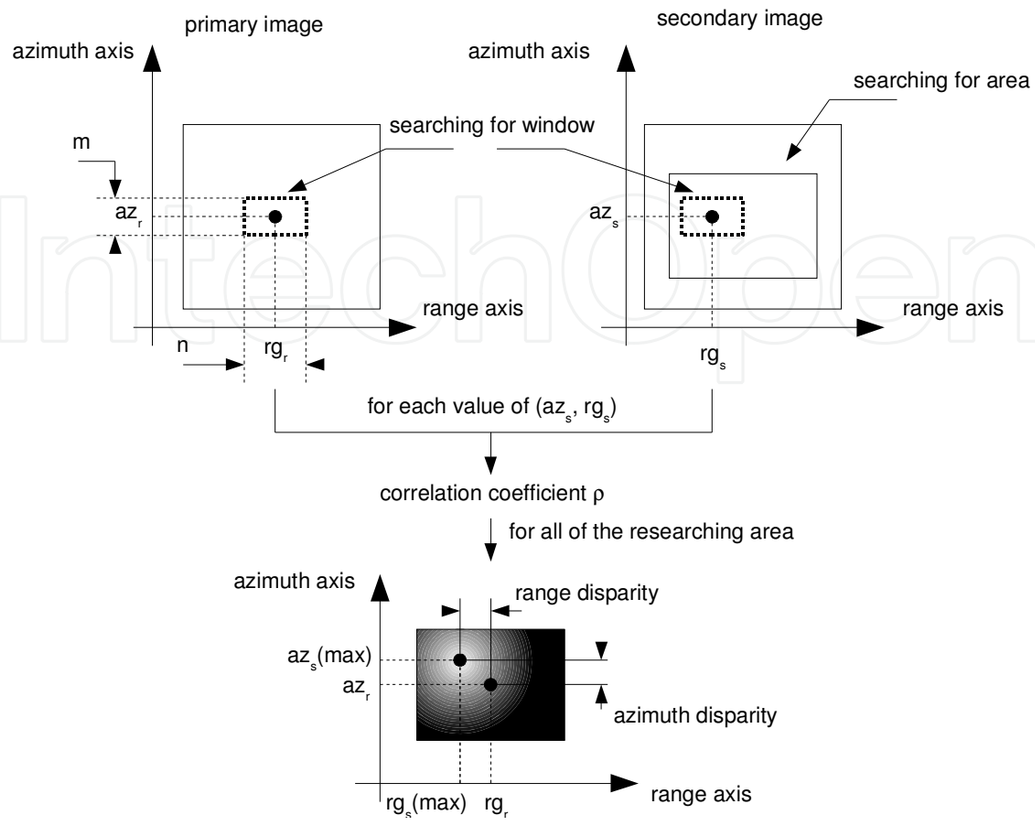

Fig. 12. Matching operations between primary image and secondary image.

3.3.3 Epipolar geometry

The use of smaller correlation windows is one way to limit the false matching result. For example, an epipolar constraint (Zhang et al., 1995) can be applied and reduce the research of the matched window along the azimuth axis. Considering parallel flight paths at a constant altitude and using the epipolar geometry, we can reduce the search area assuming that for a given point in an image, the corresponding point is located on the same azimuth line. Ideally, the search area can be reduced on a thin strip of one pixel thickness on the epipolar line. Practically, it is better to have a reduced search area one to 3 pixels wide along the azimuth axis because the estimation errors can lead to mistaken parameters. Finally, the epipolar geometry considerably reduces the size of the search area and also reduces computing time. Moreover, it limits false matching because for one pixel to match, there are fewer candidates on the other images than a larger window. The second way uses a partial knowledge of the terrain elevation that limits the research along the range axis: knowing the minimum and maximum elevation of the area, we compute the minimum and the maximum disparities along the range axis.

3.3.4 Pyramidal procedure

Another way can be considered as a hierarchical strategy used to reduce processing time and to make it possible to work with large images (Denos, 1992). The principle is quite simple:

from the original image, we build an image pyramid. At each level, the image size is reduced by a factor 2^k corresponding to the kth-iteration step. The images are reduced by transforming the pixels gray levels: in the reduced image, each pixel value corresponds to other pixels in the previous image. There are several possibilities for the transformation law: a simple one i.e the average of 4 pixels to get one pixel (see figure 13) in the reduced image or a more elaborated law i.e a Gaussian filter (Burt & Adelson, 1983) whose impulse response is given as follows:

$$w_k(u,v) = \frac{1}{2^k \sigma_I \sqrt{2\pi}} \exp(-\frac{u^2+v^2}{2^{2k}\sigma_I^2})$$

where σ_I is the standard deviation of the image $I(u,v)$. For each iteration, the matching pro-

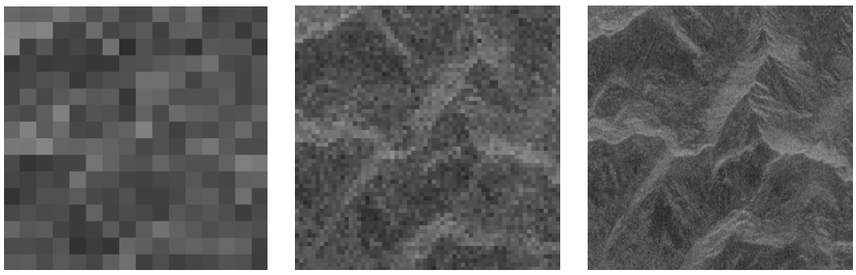

(a) : 16 x 16 (b) : 64 x 64 (c) : 256 x 256

Fig. 13. Radar images with growing resolutions: from the first step (a) to the final step (c)

cess makes it possible to establish an approximate disparity map. Thus, we are able to predict the disparity offsets at the next level of the hierarchical process, reducing computation time and speckle errors. With increasing interaction, we obtain better accuracy for each level. At the final step, the last disparity map is used to produce the Digital Elevation Model. In this way, some DEM have been produced by using very large areas such as the one computed thanks to the RADARSAT-1 data about 8,000 by 8,000 pixels.

3.3.5 Speckle filtering

As previously developed, the speckle phenomenon affects the interpretation of a radar image and is undesirable for radargrammetric applications. Speckle reduction is required prior image analysis in order to improve the use of radar images. The reduction operations called speckle filtering may be very subtle because we have to get rid of the speckle effect but not of the edges and structures in the image (figure 14). Several studies (Denos, 1992) (Jacquis, 1997) prove that speckle filtering could be efficient in order to improve radargrammetric processing. But, other works about the needs to remove the speckle effect (Dowman et al., 1993) demonstrate that speckle filtering does not improve the results of radargrammetric computation. Anyway, speckle reduction can be achieved in two ways:

- multi-look processing that refers to the division of the radar beam in N_f narrow subbeams and the result is independent as regards the speckle effect. The N_f images are summed and averaged to form the final image (Porcello et al., 1976). However, this simple method degrades the azimuth resolution by a factor of N_f,
- filtering techniques applied to the SAR image (Frost et al., 1982) (Lee, 1981) (Kuan et al., 1985) (Wu & Maître, 1990).

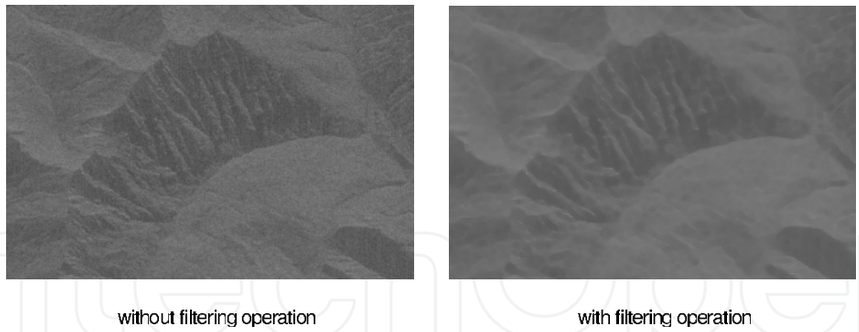

Fig. 14. Speckle filtering

The consequence of the filters on the radargrammetric performances depends on the correlation method. In our case, the computation of correlation matching based on the radar image radiometry can be improved thanks to median or Lee filters. As an overall conclusion, the filtering step is not essential to set up a radargrammetric tool kit but the application of a speckle filter to specific areas of the radar image could be beneficial in order to cancel the bad matching operations.

3.3.6 Computation of the radar stereo model

The objective of this step is to extract three-dimensional geometric data from radar stereo pairs of images by using the coordinates (position and velocity) of the satellite along the flight path. The results of such a computation is to calculate the coordinates (x,y,z) in the chosen reference as described in part 2.3.5. In the case of monocular observations, the height information h is known and we have to get the position of this point. Therefore, we can establish the system given the coordinates (x,y,z) according to the value of h of one point and the corresponding position (X_i,Y_i,Z_i) and the velocity $(\dot{X}_i,\dot{Y}_i,\dot{Z}_i)$ of the satellite indexed by $i \in 1,2$:

$$\begin{cases} (x-X_i)^2+(y-Y_i)^2+(z-Z_i)^2 &= r_i^2 \\ (x-X_i)\dot{X}_i+(y-Y_i)\dot{Y}_i+(z-Z_i)\dot{Z}_i &= 0 \\ \dfrac{x^2+y^2}{(a+h)^2}+\dfrac{z^2}{(b+h)^2} &= 1 \end{cases} \tag{3}$$

Alternatively, the binocular observations use the diversity of the vision angle to get the coordinates of the point (stereoscopic method). In the radar image, a pixel is referenced by its range and azimuth indexes. On the one hand, the range distance locates the point on a range sphere that the centre is the radar position: this is the range sphere. On the other hand, the azimuth position of a pixel can give the Doppler cone which is replaced by a plane in our case because of the null Doppler frequency at the perpendicular direction of the radar beam. The intersection of the range sphere and the Doppler plane provides two solutions but only one is obviously the right one according to the direction of the radar beam. The solution (x,y,z) of the search point satisfies the following equations system

$$\begin{cases} (x-X_1)^2+(y-Y_1)^2+(z-Z_1)^2 &= r_1^2 \\ (x-X_1)\dot{X}_1+(y-Y_1)\dot{Y}_1+(z-Z_1)\dot{Z}_1 &= 0 \\ (x-X_2)^2+(y-Y_2)^2+(z-Z_2)^2 &= r_2^2 \\ (x-X_2)\dot{X}_2+(y-Y_2)\dot{Y}_2+(z-Z_2)\dot{Z}_2 &= 0 \end{cases} \tag{4}$$

where the position $(X_{1,2}, Y_{1,2}, Z_{1,2})$ and the velocity $(\dot{X}_{1,2}, \dot{Y}_{1,2}, dotZ_{1,2})$ of the radar are required to obtain a solution. Mathematically speaking, the above system is oversized because we have 3 unknowns for 4 equations. Thus, one of the 4 equations seems to be useless. However, the choice of the unused equation is not arbitrarily made but we must base our judgement on the practical measurements (see the next part 4.4.4 and especially the *Stereoscopic localisation in the geocentric reference* section)

3.3.7 Using the disparity map

In order to obtain the relief of the scene which corresponds to the height h of each pixel of the radar image (see figures 1 and 9), we can use the disparity map which has been set up for the correlation step for a pixel which is located at the value of r_g along the range axis. Generally, we can consider the baseline B_S described by the co-ordinate B_{S_r} along the range axis and B_{S_h} along the height axis. The expression of the disparity p which is also the value of parallax is given by (Leberl, 1990):

$$p = \sqrt{r_g^2 + (H-h)^2 - H^2} - \sqrt{(r_g - B_{S_r})^2 + (H + B_{S_h} - h)^2 - (H + B_{S_h})^2} - B_{S_r}$$

where the parallax p depends on the value of r_g for a given height h. Thus, the expression of h is the root of a quadratic degree equation. In the case of parallel flight paths with the same height H of the two flight paths (e.g. B_{S_h} is null or $B_{S_r} = B_S$), the expression of h can be exhibited as:

$$h = \frac{2\,H\,B_S + 2\,H\,p - \sqrt{4\,H^2\,B_S^2 + p\,\Delta}}{p + B_S}$$

with specifying that

$$\Delta = 8\,B_S\,(H^2 - r_g^2 + r_g\,B_S) + p\,(4\,B_S^2 + p^2 + 4\,p\,B_S) + 4\,p\,(H^2 - r_g^2 + r_g\,B_S)$$

This expression can be more simple in the case of a plane front wave, which means the height of the radar H is much greater than the height h of the point and also than the parallax p:

- considering the parallax along the ground range:

$$h = \frac{p}{\cot\theta_{v1} \pm \cot\theta_{v2}}$$

- considering the parallax along the slant range:

$$h = \frac{p}{\cos\theta_{v1} \pm \cos\theta_{v2}}$$

where the sign (-) is about the same-side configuration and the sign (+) the opposite-side one. The latter expressions are used for the SIR-C configuration and are available for altitudes less than 3,000 meters. Finally, the results of a DEM can exhibit empty or inconsistent areas because of the nature of the terrain (for example low radiometric levels). In order to improve the reconstruction of an elevation model, some operations such as interpolation could be applied to known areas (for example, to constrain flatness in the case of lakes).

4. Radargrammetric experimental results

4.1 Introduction

This part is dedicated to the application of the radargrammetric operations described in the latter parts, on raw data recorded by the shuttle Endeavour during the SIR-C mission (Evans, 2006). We obtained first results by using preprocessed radar images (Fayard et al. 2006) (Fayard et al., 2007a) (Fayard et al., 2007b). Therefore, we will present in this section the DEM of a mountainous area (French Alps) obtained through radargrammetric processing.

4.2 Description of SIR-C images

For our studies, we have several images obtained by the SIR-C mission during the month of April, 1994. The interesting area is around the French and Italian Alps. For obvious reasons, we prefer to deal with mountain areas in order to get elevation information rather than urban or lake areas. Thus, the stereoscopic pair of radar images is the PR17310 and PR17429 part of flight as described in figure 15. This part is also very interesting because we can obtain

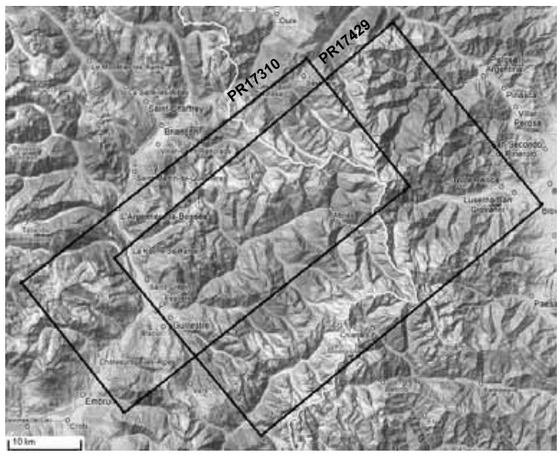

Fig. 15. Elevation map of the interesting area get from Google Maps

elevation information thanks to the IGN maps published about this region. The two flight paths are close as regards the time consideration (PR17429 on the 10th of April 1994 at 6h31 and PR17310 on the 12th of April 1994 at 5h34) so the radiometric difference due to season modifications (snow) are not present as we can see in figure 16. Moreover, the SIR-C raw data

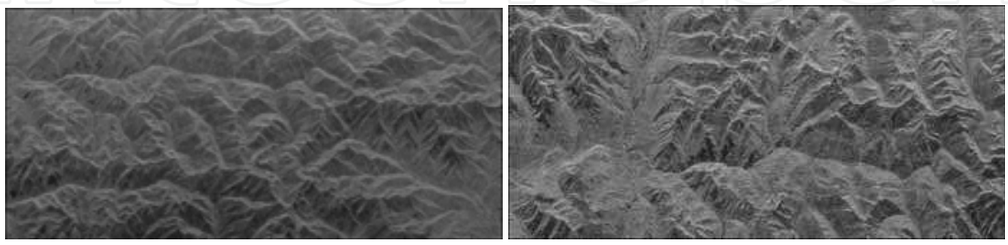

(a) SAR image from the PR17429 viewing (b) SAR image from the PR17310 viewing

Fig. 16. SAR images of the interesting area

is also recorded with the viewing parameters which are quite important for radargrammetric processing.

4.3 Preprocessing images

As it was mentioned before (part 2.3.5 about the geometrical model of the radar position), we have to describe images taking into account the co-ordinates in order to apply matching parameters. This description requires precise information about satellite trajectory.

4.3.1 Parameters of satellite tracks

In a previous section (in the part 3.3.6 about the computation of the stereo model), we drew the readert's attention to the importance of knowing the position and the velocity of the satellite during the viewing flight in order to resolve the equations (3) and (4). We cannot use the flat Earth model or strictly parallel flight in the case of raw data. Therefore, it is possible to evaluate all the positions and velocities of the satellite along its track thanks to certain viewing parameters:

- time duration τ_i defined by the time t_{init} of the beginning and the time t_{end} of the end of the recorded data,
- data sets giving the position and the velocity of the satellite at three moments t_{DS_1}, t_{DS_2} and t_{DS_3} (these moments are 4.5 seconds apart).

Thus, the interpolation of the satellite track is possible in order to link, for each pixel of the radar image, a value of the position and the velocity of the satellite along the azimuth axis. Moreover, because this interpolation is not sufficient in order to get the absolute position of radar pixels, the geocentric co-ordinates of each corner of the radar images are used to refer images to the geocentric reference. The co-ordinates of these points, latitude and longitude, are given considering the null height:

- P_{NRET} (e.g. Near Range Early Time),
- P_{NRLT} (e.g. Near Range Last Time),
- P_{FRET} (e.g. Far Range Early Time),
- P_{FRLT} (e.g. Far Range Last Time).

The figure 17 describes the geometry of the viewing path and the corresponding parameters. Also, the definition of an absolute reference for radar images is essential to get the height of the pixels and to apply epipolar transformation on radar images.

4.3.2 Epipolar resampling

In the section (part 3.3.3 about the epipolar geomtry), we moved on to the epipolar procedure that reduces the execution time for matching computation. This procedure makes it possible to limit to a thin width of az_s pixels (az_s is equal to one in theory) the search in the secondary image of the corresponding point of p_r (which is in the reference image) as can be seen in the figure 18. There are two steps to put the radar images in the epipolar geometry: forward localisation and backward localisation. For each point p_r in the reference image (e.g. #1), forward localisation is set up by using the system described by (3) and a given set of values of the height h. The result of this forward localisation is a set of points which are the solutions (x,y,z) of (3) for each value of h and a given value of r_1. We have to note that the value of r_1 is calculated thanks to the image co-ordinates az_1 (along the azimuth axis) and rg_1 (along the range axis) of a pixel and the position of the satellite corresponding to this pixel hence

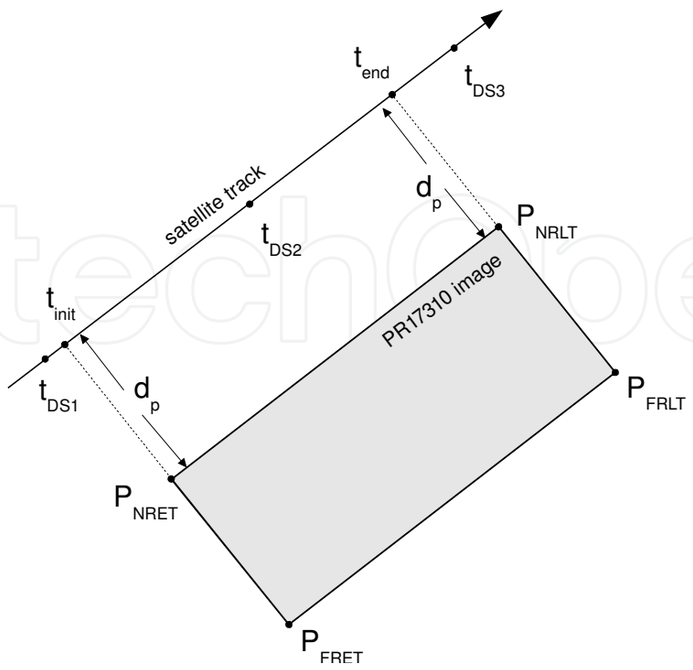

Fig. 17. Parameters of the viewing track path.

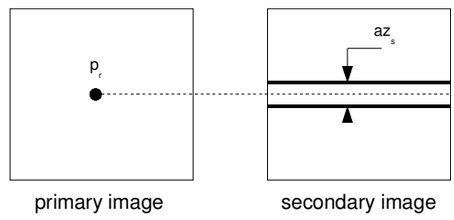

Fig. 18. Effect of epipolar geometry.

the importance of determining the satellite track parameters. Inversely, for the secondary image (e.g. #2) and from the knowledge of the height h and the co-ordinates (x,y,z) of a given point, we search for the least value of the solution r_2 of the system (3) according to the position and velocities of the satellite related to the image #2. This solution r_2 also gives the azimuth position az_2 of the corresponding pixel (because the radar beam is perpendicular to the flight path) and the calculation of the co-ordinate rg_2 is easy thanks to the value of r_2 and the radar position (X_2, Y_2, Z_2). This step is repeated for each point in the image #1 and thus the corresponding points establish the epipolar line P_s in the image #2. To obtain the epipolar line P_r in the reference image #1 from the epipolar line P_s in the secondary image #2, we have to apply the same operations i.e. forward localisation then backward localisation except that for the forward localisation from a given point of P_s, the corresponding point is calculated for only one height h_{mean}. All these operations are summarized in figure 19. In order to illustrate the achieving epipolar lines, we propose an example of epipolar line in the working area which is shown in the figure 20 from a specific point: the peak of Agrenier. This point is located in the working area by its co-ordinates az_r and rg_r in the radar image reference. For the mentioned

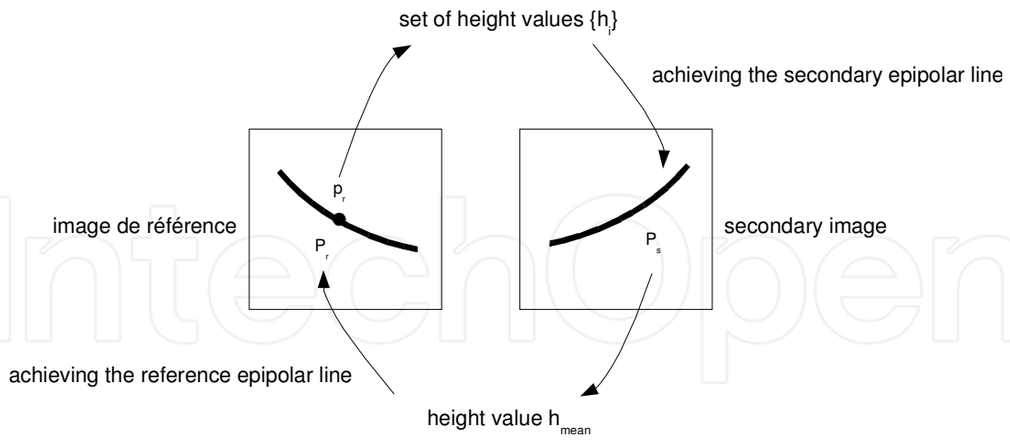

Fig. 19. Achievement the epipolar lines (reference and secondary).

Input data			Output results			
Image co-ordinates		Height	Range	Geocentric co-ordinates		
az_r (index)	rg_r (index)	h (m)	r_1 (m)	x (m)	y (m)	z (m)
1841	614	500	346,181.72	4,501,176.05	536,781.38	4,472,535.72
		1,000		4,501,729.01	537,104.25	4,472,653.93
		1,500		4,502,281.18	537,426.02	4,472,773.02
		2,000		4,502,832.56	537,746.71	4,472,892.99
		2,500		4,503,383.16	538,066.31	4,473,013.85
		3,000		4,503,932.97	538,384.84	4,473,135.57
		3,500		4,504,482.01	538,702.30	4,473,258.16
		4,000		4,505,030.27	539,018.69	4,473,381.61

Table 1. Forward localisation applied on the peak of Agrenier.

area, the IGN map gives approximately a set of heights from h_{min} = 500 meters to h_{max} = 4,000 meters. The step increment of height Δ_h is set to 500 meters thus we obtain 8 points for each value of h by the forward localisation. These points are described in the geocentric reference with the values (x, y, z) (see table 1) Also, for each output result described in table 1, we obtain the solutions r_2 and the corresponding points identified by image co-ordinates (see table 2). The output results describe the epipolar line in the secondary image (e.g. image #2) and this line is drawn in the working area of the PR17429 image in figure 21. Considering this figure, we notice the following:

1. the calculated corresponding point is on the epipolar line,
2. the calculated epipolar line does not pass through the actual corresponding point i.e. the peak of Agrenier.

The result is that the corresponding point is correctly found on the epipolar line and the accuracy of the localisation is not sufficient to retrieve the right corresponding point. Also, this inaccuracy must be corrected in order to set up the right disparity map.

4.3.3 Use of ground control points (GCP)

Because of the geode model inaccuracy, the quality of the terrain elevation reconstruction will be low. Also, we have to refine the stereo model parameters and some GCPs are required. In

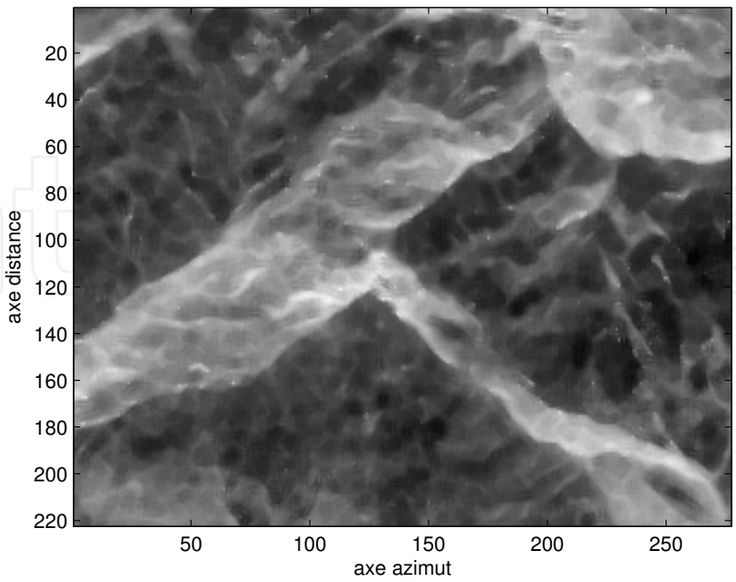

Fig. 20. Working area: PR17310 image extract

our studies, we choose 8 GCPs which cover the full terrain elevation range and are located almost at the border of the image. These GCPs are listed in table 3 just as the difference between the actual and the calculated positions of the GCPs. This comparison can be made thanks to the height information of GCPs and the forward and backward localisation operations. We note an average difference along the azimuth axis of about 6.25 pixels with a standard deviation value of 0.46 pixels and respectively 3.25 and 0.89 pixels along the range distance. So, the global correction which is applied to the secondary image reference makes it possible to recalculate the epipolar line (figure 22) that is passed through the actual corresponding point. In figure 22, we can see the search for an area about 3 pixels wide.

Input data				Output results		
Geocentric co-ordinates			Height	Range	Image co-ordinates	
x (m)	y (m)	z (m)	h (m)	r_2 (m)	az_s (index)	rg_s (index)
4,501,176.05	536,781.38	4,472,535.72	500	272,640.34	1233	239
4,501,729.01	537,104.25	4,472,653.93	1,000	272,459.73	1,232	225
4,502,281.18	537,426.02	4,472,773.02	1,500	272,279.67	1,232	212
4,502,832.56	537,746.71	4,472,892.99	2,000	272,100.16	1,231	198
4,503,383.16	538,066.31	4,473,013.85	2,500	271,921.20	1,230	185
4,503,932.97	538,384.84	4,473,135.57	3,000	271,742.78	1,229	172
4,504,482.01	538,702.30	4,473,258.16	3,500	271,564.90	1,228	158
4,505,030.27	539,018.69	4,473,381.61	4,000	271,387.57	1,228	145

Table 2. Backward localisation applied on the peak of Agrenier.

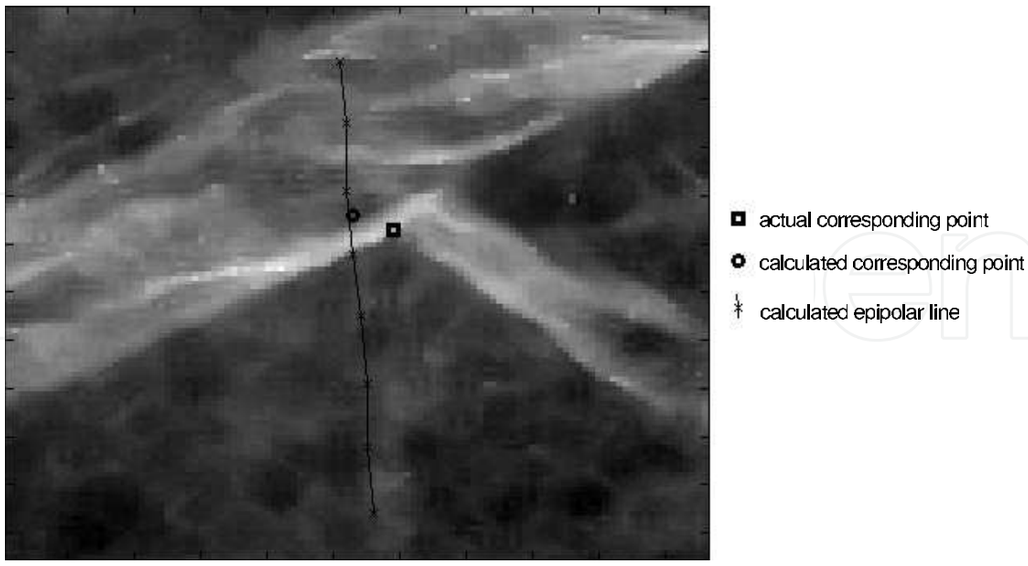

Fig. 21. Drawing the epipolar line in the PR17429 image

name of the GCP	*difference* Δaz_s	*difference* Δrg_s
Peak of Agrenier	6	3
Les Ourgières	6	3
Peak of Clapouse	7	4
Dent du Ratier	6	3
East of Col Garnier	7	5
Peak of Fond Queyvras	6	3
SE peak of Rochebrune	6	2
Top of Assan	6	3

Table 3. Difference of the co-ordinates of actual GCPs and their calculated corresponding points.

4.4 Radargrammetric processing

At this step of the entire processing, we obtain preprocessed images to which the specific radargrammetric processing will be applied: matching processing, disparity map and terrain elevation.

4.4.1 Confidence in correlation coefficient

After computing the matching operation which is described in part 3.3.2 (see the section *Correlation matching operation*), we obtain the disparity map. However, the values of disparity should be considered according to the confidence in correlation coefficient. The highest value inside a correlation surface can be perfectly detected and the corresponding position is obvious: this corresponds to a high confidence of correlation. But, this maximum position cannot clearly obtained so the confidence correlation is considered as low (see figure 23). For this case, additional noise can modify the results of the disparity map and so applying the speckle reduction and pyramidal procedure should strengthen the correlation results.

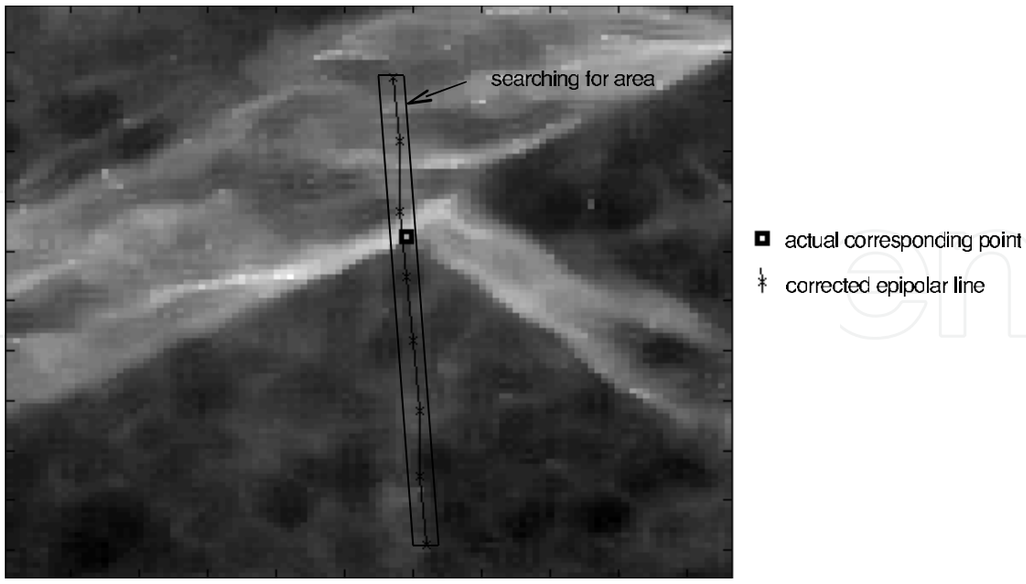

Fig. 22. Drawing the corrected epipolar line in the PR17429

4.4.2 Speckle filtering

In our application, we use two methods to reduce speckle effect. The first one is the multi-look technique which has been described before (see part 3.3.5 about the speckle filtering) and the value of N_f is equal to 4 in order not to degrade the azimuth resolution regarding the value of SIR-C parameters. Moreover, a Lee filter is applied to the radar images so the edges are preserved, which could be important considering the mountainous area. Several tests are done and the best results are obtained by using a 5 by 5 pixel window (that seems to be correct as regards the heterogeneous area). Although the speckle reduction improves the quality of the terrain reconstruction, it is not sufficient for certain areas.

4.4.3 Pyramidal computation

This method has been developed in the above section 3.3.4 and the results of this procedure will now be exposed. Firstly, we obtain the disparity map of our working area without the pyramidal steps within 50 minutes of computation using a 1.8 GHz workstation with 1GB of RAM. The resulting disparity map is described in figure 24. After that, we apply the pyramidal approach to the radar images and the resulting disparity map is obtained within 24 minutes of computation using the same workstation as before. This first consequence speaks in favour of the pyramidal scheme. Moreover, the quality of disparity map described in figure 25 is obviously better than the one in figure 24. Also, we can note two advantages of applying the pyramidal steps: computation time reduction and disparity map quality improvement.

4.4.4 Stereoscopic localisation in the geocentric reference

Thanks to the disparity map, we can reconstruct the terrain elevation by resolving the system (4). We remember this system is oversized because of 3 unknowns described by 4 equations. So, we have to choose the equation to be removed by studying the sensitivity of induced errors. This sensitivity corresponds to a correlation success when errors of about plus or minus 10 pixels are applied to the actual location of corresponding points along the azimuth axis or

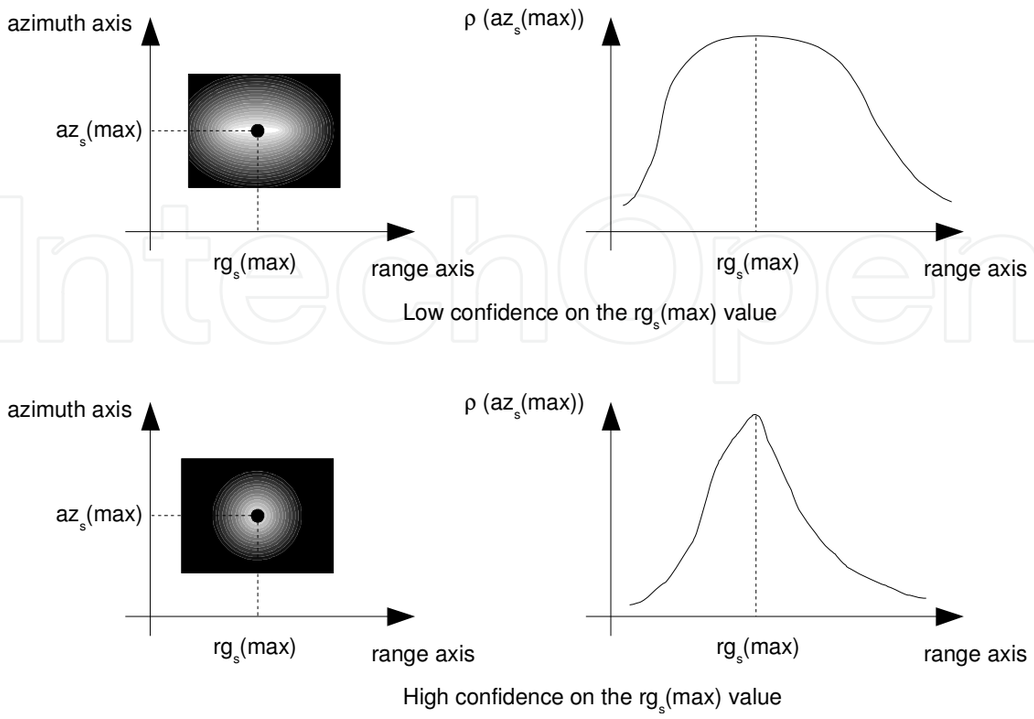

Fig. 23. Different values of confidence in correlation coefficients

	configuration #1		*configuration #2*	
	$azimuth(m)$	$range(m)$	$azimuth(m)$	$range(m)$
longitude	340	0.14	13.5	19.4
latitude	438	0.13	9.8	23.5
height	404	0.8	16	37

Table 4. RMS errors (in meters) resulting from a one pixel error in the disparity map along the azimuth axis or the range axis and considering the two configurations of the binocular system.

the range axis. Thus, by resolving 3 of the 4 equations of 4, we obtain the co-ordinates (x, y, z) which are described in the geocentric reference as latitude ϕ, longitude λ and height h and compared with the actual terrain model. The resulting error is calculated as a root-mean square operation applying to all the pixels of the working area. The results for a location error of one pixel are summarized in table 4. Two configurations of an undersized system are studied: the first one (configuration #1) uses the two iso-Doppler equations and one iso-range equation and the second one (configuration #2) uses two iso-range equations and one iso-Doppler equation. The result is obvious: it is better to chose the second configuration because an error of one pixel along the azimuth axis induces an error of less than one meter regarding the height reconstruction although the sensitivity along the range axis seems to be less in the first configuration. Another conclusion from this study is that the minimum of the correlation surface does not occur at a null shift along the azimuth and the range axis. That means this shift induce errors in the localisation and in the height reconstruction. These errors are calculated thanks to the GCPs which are used for the correction of the image indexes (see

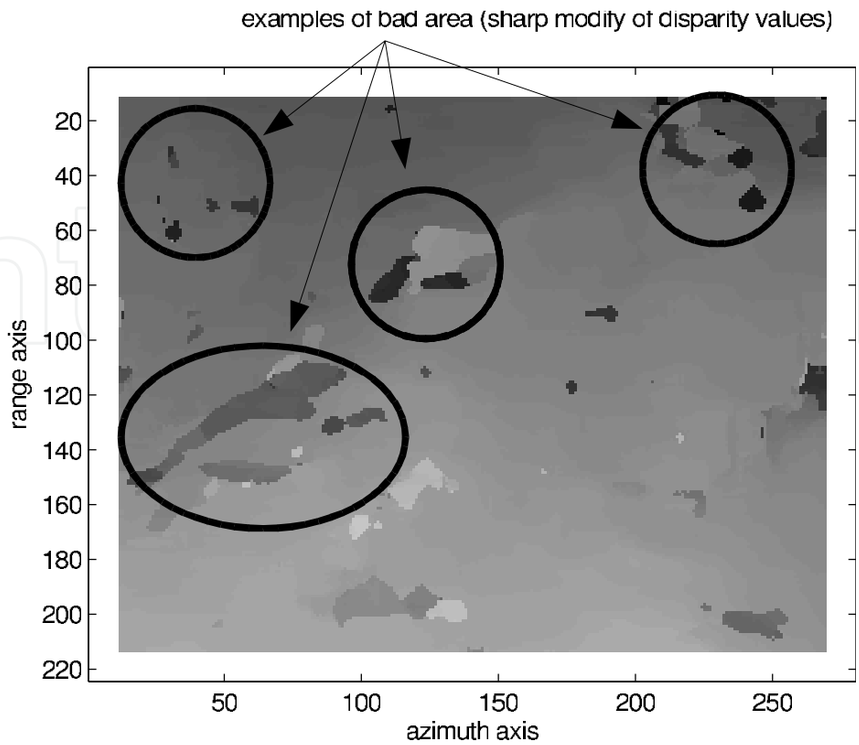

Fig. 24. Disparity map without the pyramidal procedure

section 4.3.3 about the use of ground control points). The conclusion is that the errors are less than the resolution values both for the localisation (latitude and longitude) reconstruction and for the height reconstruction.

4.4.5 Post processed DEMs

Thanks to the transformation applied at this step, we can reconstruct the terrain elevation of the working area which is seen in figure 20 by resolving the system described through configuration #2. In order to quantify the accuracy of our elevation reconstruction, we compare it with the SRTM (Shuttle Radar Topography Mission) DEM (see figure 26). We need to apply a resampling operation to our DEM because its resolution is higher than that of the SRTM . In this way, the DEM we obtain (which we can called the raw DEM) and the comparison with the SRTM DEM are shown in figure 27. The first results of the comparison are described in table 5 and show that an error of height reconstruction of less than 50 meters occurs for only 46.4 percent of pixels. Moreover, only 80 percent of pixels exhibit an error less than 200 meters. These results mean that post processing must be applied to the raw DEM. This post processing consists in removing the obvious errors which are detected by a comparison between neighbouring areas. The choice of the worked area is done thanks to an eye examination and the connected disparity is not computed to obtain the DEM. Also, the calculated DEM is not complete but more accurate than the raw one and the corresponding errors are shifted to a blank pixel (see figure 28). After removing these bad disparities, we can compare this corrected and post processed DEM with that of the STRM and the results of the comparison are described in table 5. The examination of the results shows us that more than 98 percent of pixels present

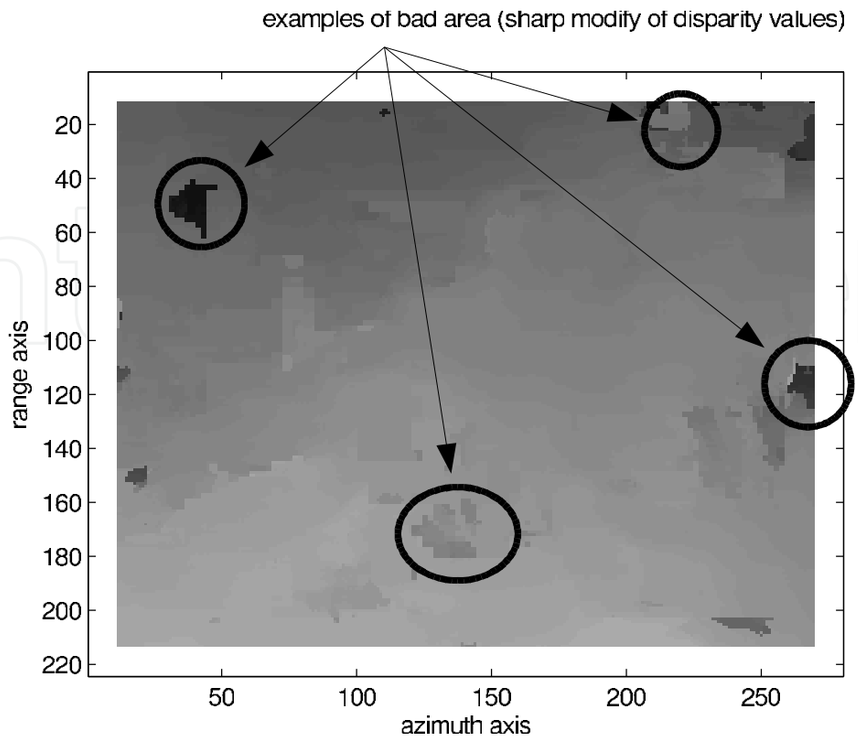

Fig. 25. Disparity map with the pyramidal procedure by using three levels of resolution

nature of DEM	number of considered points	consideration of height errors							
		< 20 m		< 50 m		< 100 m		< 200 m	
		%	ϵ_{moy}	%	ϵ_{moy}	%	ϵ_{moy}	%	ϵ_{moy}
raw DEM	2938	21.9	9.8	46.4	22.9	65.9	37.4	80.0	55.2
corrected DEM	2126	29.5	9.8	61.6	22.7	85.5	36.3	98.7	49.6

Table 5. Percent of errors and average errors ϵ_{moy} of the calculated DEMs.

an error of less than 200 meters (in comparison with the 80 percent without post computation) and the pixels whose height error is less than 50 meters are more than 61 percent (46.4 percent before). Considering the relief type and the resolution values, these results are close to the results obtained by other satellites (Toutin, 2000) (Toutin & Gray, 2000).

5. Conclusion and further developments

This chapter has dealt with the relevance of using stereoscopic radar images in order to retrieve the relief of terrain. Firstly, the basic characteristics of the radar image (SAR image) were described and the parameters which were different from those of an optical image werepointed out especially the image resolution and set up in the slant plane. Other characteristics such as the geometric and radiometric distortions were described in the rest of the section. These distortions have to be taken into account in radar stereoscopic applications in order to determine the better viewing parameters and avoid the consequences of specific radar image geometry (for example, foreshortening) and radiometry (for example, speckle effect). In the second part, we presented the radargrammetric method applied to radar images and how

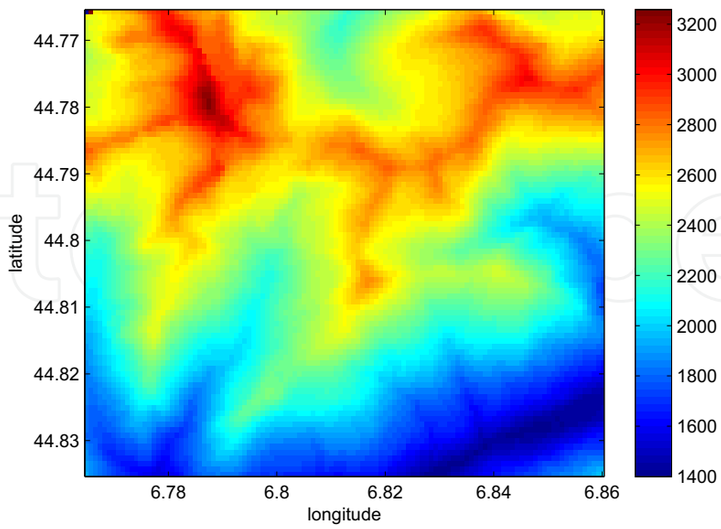

Fig. 26. SRTM DEM of the working area

they can be compared to the optical stereoscopic method. The aim of radargrammetry is to extract the height information of a radar scene from a stereo pair of radar images. Compared with the optical method, radargrammetry is based on the geometry of the visualisation flight path over the scene and the parallax induced by two views of a point characterized by its elevation. This parallax is also called the disparity between a primary image and a secondary image. The disparity is defined for each pixel in the radar image and is determined by matching computation in order to set up a disparity map. This disparity map of all the radar scenes is essential to reconstruct the height elevation by resolving a stereo-model which is described by range sphere and Doppler circle equations for each position of the radar. The accuracy of the terrain reconstruction depends on the quality of the disparity map and also on the success of the matching operation. This operation can be improved by several processing steps and especially the reduction of the speckle effect and the pyramidal approach. We can note that the geometry of the viewing scene also influences the achievement of the 3D co-ordinates of the terrain. At the end of the discussion, we illustrated radargrammetric processing by using SIR-C data over the French Alps. We showed all the steps required to obtain an acceptable DEM: from the registration of each pixel of the radar image regarding the satellite path (position and velocity) to post processing the DEM by removing the obvious bad reconstruction to choosing the better stereo-model and to using GCPs in order to refine the radar images. The resulting DEM of our radargrammetric processing is almost identical to the DEM which can be obtained thanks to specific matching and filtering operations. One of the advantages of our method is the simplicity with which an acceptable DEM is obtained.
However, it is possible to apply new methods to further improve the crucial matching step and this is what we will be working on next. We will investigate the improvement of the radargrammetric tool kit along two axes. The first one deals with the opportunities to apply some optical methods during the correlation step. Especially, the work will deal with stereo matching algorithm with an adaptive window in an SAR context. Depending on the statistical behaviour of the radar signal, we can manage the size of the correlation window in order

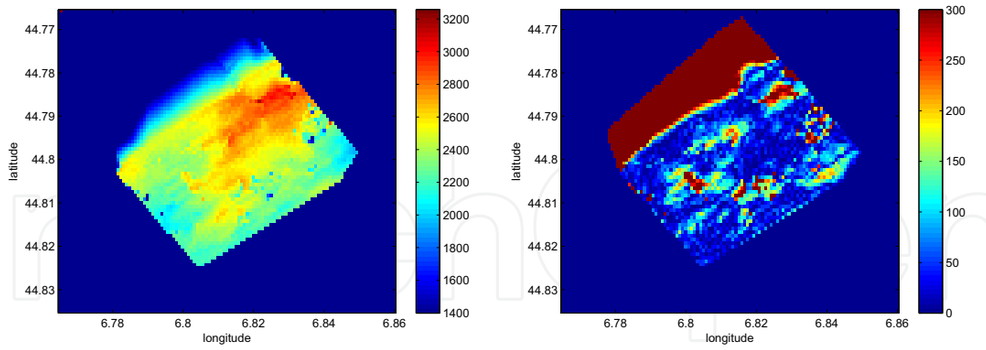

(a) Raw DEM described in the geocentric reference

(b) Difference between the raw DEM and the SRTM DEM

Fig. 27. Quantification of the raw DEM

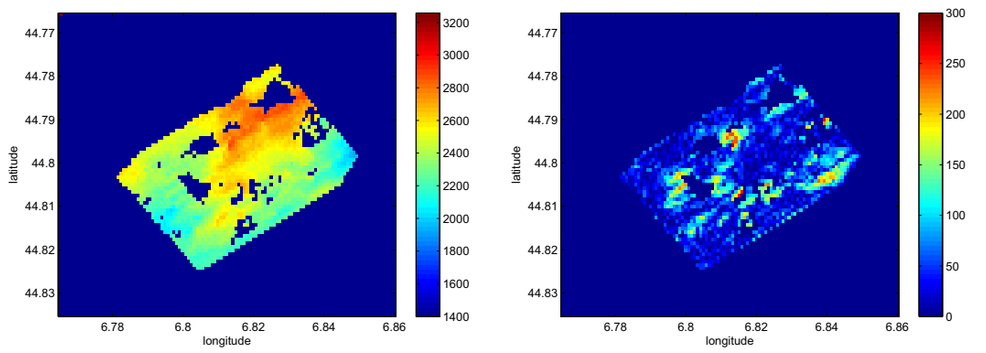

(a) Corrected DEM

(b) Difference between the corrected DEM and the SRTM DEM

Fig. 28. Quantification of the corrected DEM.

to improve the confidence of the correlation during the matching computation. The second method concerns the registration of the different areas of the image considering polarimetric parameters. Because certain areas inside an SAR image are not cooperative to the matching cooperation (e.g. shadowed or foreshortened areas), these kinds of areas could be matched together regarding the polarimetric parameters of the areas.

6. References

Beckman, P. and Spizzichino, A. (1987), *The scattering of electromagnetic waves from rough surfaces*, Artech House, 1987.

Burt, P. and Adelson, E. (1983), The laplacian pyramid as a compact image code, *IEEE Transactions on Communications*, Vol. COM-31, No. 4, pages 532–540, 1983.

Carrara, W.G., Goodman, R.S. and Majewski, R.M. (1995), *Spotlight Synthetic Aperture Radar*, Norwood, MA: Artech House, 1995.

Curlander, J.C. (1991). *Synthetic Aperture Radar, Systems and Signal Processing*. J.A. Kong, Wiley, 1991.

Denos, M. (1992), A pyramidal scheme for stereo matching SIR-B imagery, *International Journal of Remote Sensing*, Vol. 13, No. 2, pages 387 - 392, 1992.

Dhond, U.R. and Aggarwal J.K. (1989). Structure from stereo–a review. *IEEE Transactions on Systems, Man and Cybernetics*, Vol. 19, No. 6, pages 1489–1510, November 1989.

Dowman, I., Pu-Huai, C., Clochez, O. and Saundercock, G. (1993), Heighting from stereoscopic ERS-1 data, in *proceedings Second ERS-1 Symposium*, pages 609–614, 1993.

Dufour, J.P. (2001). *Introduction to geodesy*. Hermès, 2001.

Evans, D.L. (2006), Spaceborne imaging radar-C/X-band synthetic aperture radar (SIR-C/X-SAR): a look back on the tenth anniversary, *IEE Proceedings on Radar, Sonar and Navigation*, Vol. 153, No. 2, pages 81–85, 2006.

Fayard, F., Méric, S. and Pottier, E. (2006), First studies on a radargrammetric tool kit, *European conference on Synthetic Aperture Radar*, EUSAR'06, Dresden, 2006.

Fayard, F., Méric, S. and Pottier, E. (2007a), Matching stereoscopic SAR images for radargrammetric applications, *IEEE International Geoscience and Remote Sensing Symposium*, IGARSS 2007, pages 4364 - 4367, 2007.

Fayard, F., Méric, S. and Pottier, E. (2007b), Mise en appariement d'images SAR stéréoscopiques, *Journées Nationales des Micro-ondes*, JNM'07, Toulouse, 2007

Frost, V.S., Stiles, J., Shanmugan, K. and Holtzman, J. (1982). A model for radar images and its application to adaptive digital filtering of multiplicative noise, *IEEE Transactions on Pattern Analysis and Machine Intelligence*, Vol. PAMI-4, No. 2, pages 157 - 166, March 1982.

Girard, M.C. (2003). *Processing of remote sensing data*, Taylor and Francis, France.

Goodman, J.W. (1976). Some fundamental properties of speckle. *Journal of the optical society of America*, Vol. 66, No. 11, pages 1145–1150, November 1976.

Gracie, G. et al, (1970). Stereo Radar Analysis, *US Engineer Topographic Laboratory*, Report No FTR-1339-1.

Horn, B. (1975), *The psychology of computer vision–Chap. 4: obtaining shape from shading information*, Mac-Graw Hill, 1975.

Jacquis, F. (1997), *Techniques de corrélation pour la radargrammétrie — Filtrage et détection de structures — Application à des images satellites ROS-ERS1*, PhD dissertation, Joseph Fourier university, Grenoble, 1997.

Kuan, D.T., Sawchuk, A.A., Strand, T.C. and Chavel, T. (1987), Adaptive restoration of images with speckle, *IEEE Transactions on Acoustics, Speech and Signal Processing*, ASSP-35, No. 3, pages 373–383, 1987.

Leberl, F. (1990). *Radargrammetric image processing*, Artech House, Norwood, MA.

Lee, J.S. (1981), Refined filtering of image noise using local statistics, *Computer Graphics and Image Processing*, No. 15, pages 380 - 389, 1981.

La Prade, G. (1963). An analytical and experimental study of stereo for radar. *Photogrammetric Engineering*, Vol. 29, No. 2, pages 294-300.

Marr, D., Poggio, T. (1980), A theory of edge detection, *Proc. Royal Society of London*, pages 283–287.

Massonnet, D. and Rabaute, T. (1993), Radar interferometry: limits and potential, *IEEE Transactions on Geoscience and Remote Sensing*, Vol. 31, No. 2, pages 455–464, 1993.

Paillou, Ph. and Gelautz, M. (1999), Relief reconstruction from SAR stereo pairs: the " optimal gradient" matching method, *IEEE Transactions on Geoscience and Remote Sensing*, Vol. 37, No. 4, pages 2099–2107.

Polidori, L. (1997). *Cartographie radar*, Gordon and Breach Science, France.

Porcello, L., Massey, N., Innes, R. and Marks J. (1976). Speckle reduction in synthetic aperture radar, *Journal of the Optical Society of America*, Vol. 66, No. 11, pages 1305–1311, 1976.

Rosenfield, G.H., Stereo radar techniques, *Photogrammetric Engineering*, Vol. 34, pages 586-594.

Schreier, G (1993). *SAR Geocoding: data and systems*, (18 papers) Wichmann Verlag, Karlsruhe, Germany.

Schuler, D.L., Lee, J.S. And De Grandi, G. (1996), Measurement of topography using polarimetric SAR images, *IEEE Transactions on Geoscience and Remote Sensing*, Vol. 34, No. 5, pages 1266–1277, 1996.

Sylvander, S., Cousson, D. and Gigord, P. (1997), Etude des performances géométriques des images RADARSAT, *Bulletin de la société Française de Photogrammétrie et de Télédétection 148*, pages 57–65.

Toutin, T. (2000), Evaluation of radargrammetric DEM from RADARSAT images in high relief areas, *IEEE Transactions on Geoscience and Remote Sensing*, Vol. 38, No. 2, pages 782–789, 2000.

Toutin, T. and Gray, L. (2000), State-of-the-art of elevation extraction from satellite SAR data, *ISPRS Journal of Photogrammetry and Remote Sensing*, Vol. 55, pages 13–33, 2000.

Toutin, T. (2006). Generation of DSMs from SPOT-5 in-track HRS and across-track HRG stereo data using spatiotriangulation and autocalibration. *ISPRS Journal of Photogrammetry and Remote Sensing*, Vol. 60, No. 3, May 2006, pages 170–181.

Ulaby, F.T. (1981), *Microwave remote sensing, active and passive*, Artech House, 1981.

Wu, Y. and Maître, H. (1990), A speckle suppression method for SAR images using maximum homogeneous region filtering, in *IGARSS'90*, Vol. 3, pages 2413–2416, 1990.

Zhang, Z., Deriche, R., Faugeras, O. and Luong, Q.T., A robust technique for matching two uncalibrated images through the recovery of the unknown epipolar geometry, *Artificial intelligence*, Vol. 78, pages 87–119, 1995.

Geoscience and Remote Sensing

Edited by Pei-Gee Peter Ho

ISBN 978-953-307-003-2
Hard cover, 598 pages
Publisher InTech
Published online 01, October, 2009
Published in print edition October, 2009

Remote Sensing is collecting and interpreting information on targets without being in physical contact with the objects. Aircraft, satellites ...etc are the major platforms for remote sensing observations. Unlike electrical, magnetic and gravity surveys that measure force fields, remote sensing technology is commonly referred to methods that employ electromagnetic energy as radio waves, light and heat as the means of detecting and measuring target characteristics. Geoscience is a study of nature world from the core of the earth, to the depths of oceans and to the outer space. This branch of study can help mitigate volcanic eruptions, floods, landslides ... etc terrible human life disaster and help develop ground water, mineral ores, fossil fuels and construction materials. Also, it studies physical, chemical reactions to understand the distribution of the nature resources. Therefore, the geoscience encompass earth, atmospheric, oceanography, pedology, petrology, mineralogy, hydrology and geology. This book covers latest and futuristic developments in remote sensing novel theory and applications by numerous scholars, researchers and experts. It is organized into 26 excellent chapters which include optical and infrared modeling, microwave scattering propagation, forests and vegetation, soils, ocean temperature, geographic information , object classification, data mining, image processing, passive optical sensor, multispectral and hyperspectral sensing, lidar, radiometer instruments, calibration, active microwave and SAR processing. Last but not the least, this book presented chapters that highlight frontier works in remote sensing information processing. I am very pleased to have leaders in the field to prepare and contribute their most current research and development work. Although no attempt is made to cover every topic in remote sensing and geoscience, these entire 26 remote sensing technology chapters shall give readers a good insight. All topics listed are equal important and significant.

How to reference

In order to correctly reference this scholarly work, feel free to copy and paste the following:

Stephane Meric, Franck Fayard and Eric Pottier (2009). Radargrammetric SAR Image Processing, Geoscience and Remote Sensing, Pei-Gee Peter Ho (Ed.), ISBN: 978-953-307-003-2, InTech, Available from: http://www.intechopen.com/books/geoscience-and-remote-sensing/radargrammetric-sar-image-processing

INTECH
open science | open minds

InTech Europe
University Campus STeP Ri
Slavka Krautzeka 83/A
51000 Rijeka, Croatia

InTech China
Unit 405, Office Block, Hotel Equatorial Shanghai
No.65, Yan An Road (West), Shanghai, 200040, China
中国上海市延安西路65号上海国际贵都大饭店办公楼405单元

www.intechopen.com

Phone: +385 (51) 770 447
Fax: +385 (51) 686 166
www.intechopen.com

Phone: +86-21-62489820
Fax: +86-21-62489821

IntechOpen

IntechOpen